REVIEW ARTICLE

State-of-the-art MEMS and microsystem tools for brain research

John P. Seymour[1], Fan Wu[2], Kensall D. Wise[1,3] and Euisik Yoon[1,3]

Mapping brain activity has received growing worldwide interest because it is expected to improve disease treatment and allow for the development of important neuromorphic computational methods. MEMS and microsystems are expected to continue to offer new and exciting solutions to meet the need for high-density, high-fidelity neural interfaces. Herein, the state-of-the-art in recording and stimulation tools for brain research is reviewed, and some of the most significant technology trends shaping the field of neurotechnology are discussed.

INTRODUCTION

'Neuroscience today is like chemistry before the periodic table: People knew about elements and compounds but lacked a systematic theory to classify their knowledge.' –Paul Allen and Francis Collins, Wall Street Journal, 2013 (Ref. 1).

The lack of a systematic theory of neural activity is complicated by the scale of the human brain, with an estimated 85 billion neurons, 100 trillion synapses, and 100 chemical neurotransmitters[2]. Understanding what makes any one neuron fire, or not fire, is a central question in neuroscience, and thus, the ideal sensing tool must span from the single neuron to its complex network of connections if we are to understand how a particular 'cell type' assimilates information[3,4]. In doing so, neuroscientists will identify new circuit 'elements' or neuronal cell types that may someday provide the world with a general theory of brain activity[5,6], similar to how the periodic table arose from the study of repeating physical properties. Microelectromechanical systems (MEMS) and microsystems have enabled the study of neurons from the single unit to the scale of large populations, and all indications are that these technologies will continue to be an important tool-making platform for the neuroscience community.

Since the 1950s, recording capacity has been steadily increasing through the use of improved microelectrode technology, but this technology alone has not yielded the fundamental breakthroughs required to thoroughly understand the cellular components of a neuronal circuit. Beginning in 2005, seminal studies on optogenetics introduced methods for exciting and inhibiting neurons in ways specific to genetic and chemical markers of a particular cell type[7,8]. Optical control of genetically engineered ion channels is a powerful tool for parsing circuit elements and cell types in the dense heterogeneous populations surrounding a microelectrode recording site[4,9]. Biotechnologists are rapidly discovering new opsins (light-activated ion channels)[10–12], and neurotechnologists are racing to scale light-delivery instruments,

while simultaneously scaling electrical recording capabilities in the illuminated regions of tissue. Like optogenetics, other novel means of neuron control are beginning to be used, especially in the form of small molecules either 'caged' and released with local light stimulation[13] or with receptor-specific ligands that can be controlled temporally and locally with other drugs (commonly called DREADDs for designer receptors exclusively activated by designer drugs)[14,15]. The contribution that microscale devices can make to these latest biology tools is still unproven but certainly intriguing given the many delivery, sensing, and actuation modalities that can be applied.

The potential to generate breakthroughs in mapping brain activity has prompted many governmental and non-governmental agencies to invest in new tools. The Human Connectome Project, an early mapping initiative, began in the United States in 2010 and emphasized macroscale anatomical connections. Europe's Human Brain Project is a 10-year program that began in 2013 and increased the focus on supporting neurotechnology development for functional mapping in animals and humans. President Obama's 'brain research through Advancing Innovative Neurotechnologies' (BRAIN) Initiative began funding research in 2014, with funding also tailored toward technology development for functional mapping and microscale neural circuit reconstruction. Japan announced their own program, Brain/MINDS, in October 2014, which is specializing in mapping activity in a marmoset animal model. An important aspect of brain mapping technology is that it should also be compatible with awake behavioral studies, which will require considerable advances in miniaturization and packaging. This surge in investment worldwide will have long-term benefits for all societies by improving the understanding of neurological diseases, which are the cause of 6.8 million deaths annually[16]. Beyond the obvious health benefits, insight into how animals and humans self-learn and perform pattern recognition will inform the burgeoning field of neuromorphic computing[17,18]. Neuromorphic computing is a biomimetic architectural approach

[1]Department of Electrical Engineering and Computer Science, University of Michigan, Ann Arbor, MI 48105, USA; [2]Diagnostic Biochips, Inc., Glen Burnie, MD 21061, USA and [3]Department of Biomedical Engineering, University of Michigan, Ann Arbor, MI 48105, USA.
Correspondence: Dr J Seymour (seymourj@umich.edu)

that is replacing the von Neumann architecture with highly parallel, analog processing to achieve brain-like energy efficiency and adaptability. Systems neuroscience knowledge gleaned from neurotechnology will disrupt the microprocessor industry, while creating powerful new research tools and consumer products.

This paper will review recent developments in MEMS and microsystems for large-scale sensing and perturbation of brain activity with a focus on electrical recording and optical stimulation modalities. Electrical recording methods provide the greatest temporal resolution and frequency range and complement genetically targeted optical stimulation. New modalities also have the potential to contribute and perhaps displace electrical approaches in some applications. Two nascent implantable technologies include optical recording devices and optical stimulation, both used in conjunction with genetic modification to enable either an optical to ionic transduction or an ionic to optical transduction. Finally, despite modest improvements in microsystem density and integration in the last decade, we present encouraging trends in high-density circuit architecture and packaging.

RECORDING BRAIN ACTIVITY
Brief history
The intracellular electrode was fundamental to understanding the action potential and remains the gold standard for understanding single-cell neurophysiology[19–21], but it is difficult to scale and is damaging to the cell. The extracellular electrode, which can electrically record the signature of several neuronal action potentials, proved to be another major breakthrough because an array can sense a large number of single-neuron action potentials with limited disruption to the local circuit. The extracellular microelectrode (Figure 1) penetrates the brain and has a recording range of 65 (Ref. 22) to 150 μm (Ref. 23). Importantly, this electrode can capture 'single-unit activity' or 'spikes' in the context of population dynamics and thus was the first technology capable of circuit mapping[24]. Microwires were the first such devices and have been an effective research tool for studying the brain for nearly 60 years (Refs. 25,26). Microwires evolved into stereotrodes and tetrodes[22,27] with a variety of insulating and conductor materials depending on the recording or stimulation requirements. Electrode measurements approximate the superposition of voltages from a series of monopolar current sources in the local tissue, derived from Ohm's law,

$$V = \sum_{i=1}^{n} \frac{I_i}{4\pi\sigma r_i} \qquad (1)$$

where I_i is the current of one point source, σ is the conductivity of the extracellular space, and r_i is the distance from the source to the electrode (a dipole assumption results in a more complex isopotential and an amplitude proportional to $1/r^2$, but arguably the ratio is neither a monopole or dipole[28–31]). Given the close spacing of tetrodes, multiple spike signals can be used to triangulate and localize a specific cell in space[32].

The pioneering work of Wise at Stanford University[33,34] and at the University of Michigan[35,36] in developing microfabricated silicon electrode arrays was a major advancement. The geometrical precision of lithographic techniques has allowed neuroscientists to imagine unique electrode designs having unprecedented site density. In 1982, engineers first used selective boron doping of microelectrode silicon probes to create wet etch-stops in a technique that produced smooth needle-like structures ideal for minimizing tissue damage[37]. This technique spread throughout the MEMS community and formed the basis for many other novel electromechanical structures. The planar lithography approach has evolved over the years to include integrated interconnects[38], active electronics[35,39,40], cochlear implants[41,42],

polytrodes[31], and three-dimensional arrays[29,43–45]. An important simplification for defining and releasing fine neural probe structures has been the use of silicon-on-insulator (SOI) wafers and deep reactive ion etching (DRIE)[46,47] that many groups have adopted.

Another MEMS technology that has redefined the microelectrode is the 'Utah' array, originally developed by the Normann group at the University of Utah[48–50]. The 'Utah' array is generally fabricated as a 10-by-10 array of tines machined from 3-mm-thick silicon wafers. These tines are anisotropically etched and doped to form a monolithic array of conductive needles. Lithography is used on the backend to define bonding pads with one channel per tine. This approach provides robust mechanical properties that have made it very popular in primate research[51–54]. This silicon electrode platform has been the basis for successful human trials using a brain machine interface[55–57] and has been adapted by several groups for wireless integration[58–60].

Another form of high-density recording arrays is surface arrays, either for *in vitro* or *in vivo* experiments. Surface arrays for tissue slices and retinal recording are known as multi-electrode arrays (MEAs). Electrical recording with MEAs from the retina or hippocampal slices has provided the highest density of information available, in part because there is no requirement for miniaturization on the backend. Despite the lack of physical constraints, certain MEA architectures have achieved unprecedented miniaturization, as discussed in Subsection 'High-density active recording' below. Commercial MEAs containing tens of thousands of electrode channels provide remarkable resolution of neural activity spreading over time, often referred to as electrical imaging, and have been designed for tissue culture and slices. MEAs are usually CMOS devices with relatively simple post-CMOS metallization. Several reviews on *in vitro* or MEA approaches are available[61–63]. However, nanoscale MEMS-based processing is increasingly being developed to achieve intracellular recordings in particular[64–66]. We will return to the topic of MEAs because advances in wafer thinning, chip integration, and flexible electronics are blurring the line between *in vitro* and *in vivo* devices.

Surface recordings on the brain record an electrocorticoencephalogram (ECoG) and are often referred to as ECoG arrays or microgrids. These arrays are effectively flexible versions of MEAs. ECoG arrays are less invasive than microelectrodes and have higher spatial resolution[67] than electroencephalogram (EEG) arrays, which is limited to signals spatially filtered by the dura and skull (Figure 1). Macroscale versions of an ECoG array are generally platinum discs soldered to metal wires and molded in medical grade silicone or polyurethane. These devices exist commercially, but a significant push toward microscale structures has revealed important physiological data that neuroscientists have embraced[23,68]. Advancing ECoG and EEG electrodes and their microsystems will be particularly useful for conducting neuroscience and neurology studies in human patients.

ECoG and microECoG are the best surface array methods for source localization, but recent advances in EEG source localization when accounting for patient-specific anatomy and conductivities now claim sub-cm^2 resolution[69]. Technology improvements for EEG systems have also witnessed an increase in funding, including those made at the Army Research Laboratory in the United States, with the goal of making EEG a practical tool for widespread human-based neuroscience in real-world applications[70]. EEG systems will benefit from microscale electrode features such as microneedle electrode designs that reduce the variability in skin contact[71] and mixed-signal front-ends with reduced size and power to eliminate long analog wires.

Advantages and challenges of high-density recording arrays
Systems neuroscience is seeking to monitor single-neuron activity in the context of very large populations to identify how the
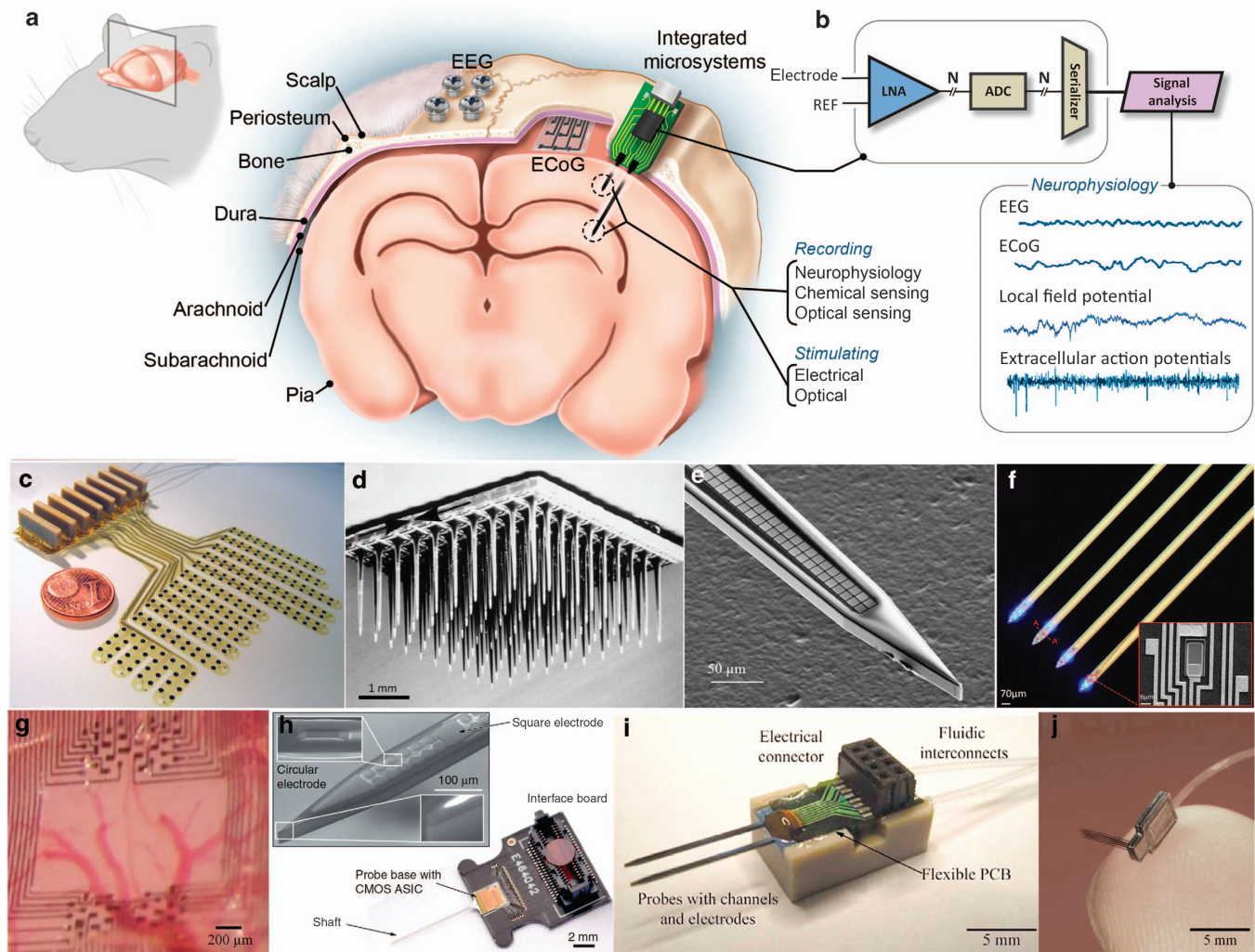
Figure 1 Recording and stimulating technologies vary across scale and degrees of invasiveness. (**a**) Illustration of the rodent brain and a variety of technologies from electroencephalogram (EEG) to intracortical microelectrodes. (**b**) High-density systems will increasingly require built-in active electronics to serialize large data streams and reduce the size of the connectors. Sample electrical signals show the amplitudes of various signal sources. The intracortical arrays are often microelectrodes but may also include chemical and optical sensors. (**c**) Polyimide electrocorticogram (ECoG) for large area mapping[67]. (**d**) A "Utah array" with 400 µm shank spacing and 100 channels has been used in human studies[50]. (**e**) Close-packed recording sites with 9×9 µm area and a pitch of 11 µm[178]. (**f**) MicroLED optoelectrode made from GaN on silicon[176]. (**g**) Parylene ECoG with greatly improved resolution over EEG and even single-cell capabilities[23]. (**h**) CMOS integration on probe shaft and backend[40]. (**i**) Fluidic probe for drug delivery[45]. (**j**) Active 3D silicon recording system with flexible parylene interconnect[182].

constituent parts lead to the emergent properties of the whole. The number of simultaneously recorded neurons has been doubling approximately every 7 years (Refs. 72,73). Additional investment in brain mapping technology is ongoing and justified because even at this rate of doubling we are still far from achieving recording densities capable of whole-brain mapping[6,74]. Although new optical imaging and recording modalities will certainly accelerate this rate of discovery, electrical recording methods still provide the greatest temporal resolution and frequency range. Many neuroscientists continue to rely on the simultaneous measurement of single-cell spiking and local field potentials (which includes delta, theta, alpha, beta, spindle bursts, and gamma oscillations) to derive complex network effects[75]. Tetrodes (four wires closely spaced together) continue to be the workhorse of electrophysiology because they are often fabricated in research labs at low cost. However, neuroscientists have increasingly found it efficient to use high-density microfabricated electrodes. Microfabricated arrays offer a large design space and geometric precision and can at least match the two-dimensional

cellular density of the brain over a greater span than that observed for tetrodes. Three other compelling advantages of microfabricated recording arrays are also worth noting. First, overlapping recording regions can form multiple tetrodes or polytrodes and have proven the best means for maximizing single-cell identification on a per-channel basis. Microstructures of various materials and geometries also offer ways to minimize adverse tissue reactions. Finally, the integration of MEMS-based probes with actuators and amplifier microsystems will provide more effective tools for brain mapping (discussed in Sections 'STIMULATING BRAIN ACTIVITY' and 'SCALABLE IMPLANTABLE MICROSYSTEMS', respectively). Despite all of these advantages, several key remaining challenges should be addressed.

The recording of spikes in a mammalian brain is as much a software challenge as it is a hardware one. Thermal, electrical, and biological noise sources can combine to severely limit the signal-to-noise ratio[76,77] and, when combined with spiking variability, can result in false spike detection, missed detection, and erroneous classifications[78,79]. Despite >50 years of advances and a

plethora of algorithms for addressing issues of accuracy and speed, neuroscientists, mathematicians, and technologists are still far from reaching the goal of real-time automated spike sorting[30,80]. The stereotrode[27] and tetrode[22] were hardware solutions designed to help address the problem of spike sorting accuracy. Overlapping recording regions to maximize confidence in a putative action potential was first recognized using two twisted microwires measuring 20 μm in diameter and spaced only a few microns apart[27]. In one study, a MEMS-based array with a linear tetrode was validated using intracellular recordings as 'ground truth' for spike sorting. Tetrode versus single-site recordings yielded both greater accuracy and greater numbers of units per channel[78]. Another study extended this logic and used a dense 2D array of 54 channels on 1 shank to compare the performance of virtual tetrodes (grouping four adjacent electrodes) and polytrodes (more than four electrodes). The authors' data were limited to relatively large site pitches (43–65 μm) but showed that polytrodes outperformed even tetrodes in isolating multi-unit clusters into individual single units[31]. This same study also found as many as 24 single units in a virtual tetrode in the relatively sparse visual cortex. More recently, software algorithms that utilize precise spatial information as part of the sorting logic show great promise for improving both speed and accuracy[30,80–82]. Investigating the optimal microelectrode size and pitch for speed and accuracy in spike sorting is an important research area.

Accurate real-time automated spike sorting is still unproven but will be a heralded breakthrough in systems neuroscience and in clinical applications such as neural prostheses requiring a brain-machine interface. Using MEMS-based arrays to improve software tools for neuroscientists also involves neuronal location information[9,24,29,31] and cell classification of neurons[4,83], which are critical in brain mapping. The need for technologies to enable cell typing in brain research was highlighted as the number one priority by the U.S. BRAIN Initiative[84], and combining recording techniques with genetically targeted methods such as optogenetics and pharmacogenetics[85] is expected to make cell typing more reliable[6]. MEMS-based devices can certainly provide the resolution if this expectation proves to be the enabling requirement for new software tools, but device reliability and micro-sized packaging solutions are significant constraints that must be part of the solution.

Tissue response and structure size

The adverse tissue response to implantable neurotechnology has been an ongoing area of active research and is reviewed elsewhere (Jorfi, Capadonia 2015)[86]. Important components of the adverse response have been studied, including insertion trauma[87–89], the intrinsic foreign body response[90,91], and strain-induced damage from mechanical mismatch[92–94]. Long-term reliability is clearly more of a challenge in clinical applications than for neuroscience; nonetheless, tools for brain mapping should be designed to minimize disruption to the circuits being investigated. The size of the device placed into spinal cord or brain tissue undoubtedly affects the degree of initial damage. The mean distance from the center of a neuron (somatic center) to the nearest microvasculature is only 15 μm (Ref. 95); thus, regional damage to the blood–brain barrier is unavoidably a function of size[88]. The intrinsic foreign body response is complex and intertwined with the issue of micromotion, which is related to mechanical factors such as the probe cross-sectional area, lattice or porous architecture, total surface area, and stiffness. Biochemical factors may include material stability, chemical properties, and protein adhesion. Work on these mechanical factors will be briefly reviewed here because MEMS allow for the selection of a large range of materials and geometries.

There is mixed evidence indicating that geometric size is an important design criteria in achieving reliable high-density recordings (Figure 2). Evidence from several groups indicates that when small features are used there is a significant improvement in many histological markers, but whether those are the best markers to predict performance is unclear. In early studies on geometry, differences in relatively large structures resulted in similar long-term outcomes[96,97]. When cellular-scale probe thickness dimensions (5 μm) were compared against the dimensions of a polymer shank (~50 μm), however, there was a significant difference in non-neuronal density (300% higher at the shank) and neuronal density (40% lower at the shank) in favor of smaller structures[98] (Figure 2a). Qualitatively, the interface around the 5 μm edge also showed improvement in microglia and astrocyte reactivity. Two other studies independently supported these results using different materials and elastic moduli, with similarly small feature sizes[99–101]. Silicon was used to make a lattice probe with exceptionally fine features[102,103] measuring 5 μm that was implanted and reduced a variety of glial reactive markers[99,104]. The most creative application of the lattice structure was recently demonstrated by creating an injectable SU-8-based lattice inserted through a 22-gauge needle and electrically connected to a printed circuit board (PCB) using anisotropic conductive film during surgery[105]. Although histological evidence supports the use of smaller, lattice-like structures, no group has yet provided strong evidence that reliable single-cell resolution can be achieved across many channels for more than even one year. Currently, the gold standard among neuroscientists seeking long-term single-cell recording is the use of a microdrive to periodically 'tune' the position of silicon neural probes (particularly those with thicknesses ranging from 12 to 15 μm and shanks measuring approximately 60 μm wide for rodent studies)[106]. Therefore, interest in and funding for advanced microelectrodes have been increasing given both the current success and the potential for further improvements of large-scale long-term electrophysiology.

Substrate materials and microfabrication

A variety of materials and methods have been explored for use in neural probes. Figure 3 highlights seminal studies on novel substrates and compares the substrates' intrinsic stiffness. Each of these substrate materials has shown good biostability, albeit with varying degrees of evidence, but many other properties must also be considered in the context of the application at hand, including the practical processing questions regarding deposition, etching, adhesion, and general process compatibility. Many substrate materials have been explored to date, providing researchers an excellent toolbox.

Substrates can be classified as inorganic (for example, silicon[33], titanium[107], diamond[108], zinc oxide[109], and silicon carbide[110]) or organic (for example, carbon fiber[101], parylene[111,112], SU-8[105,113], polyimide[114,115], and silicone[116]). Silicone, which includes polydimethylsiloxane (PDMS), is an important class of silicon-based organics that provides a useful range of properties, particularly elasticity, not otherwise available. Brain tissue elasticity is still two orders of magnitude lower than the softest PDMS currently being used (not including Ecoflex® or gels, Macungie, PA, USA). Nonetheless, useful devices have been demonstrated on either end of the modulus spectrum, with stiffer materials enabling robust micron-sized structures and elastic materials enabling stretchable substrates at the expense of thickness or requiring the use of insertion aids. PDMS, the best known of the silicones, has proven amazingly versatile in the microfluidics and medical device communities but has found limited use in thin-film devices. The primary challenges have been metal adhesion and creating thin substrates, although improvements are forthcoming[117,118]. Important work reported by Minev et al. (Ref. 116) recently demonstrated that PDMS is an effective substrate for stimulation and drug delivery. As the feature size improves, the material may become equally useful for high-density recording. Even more
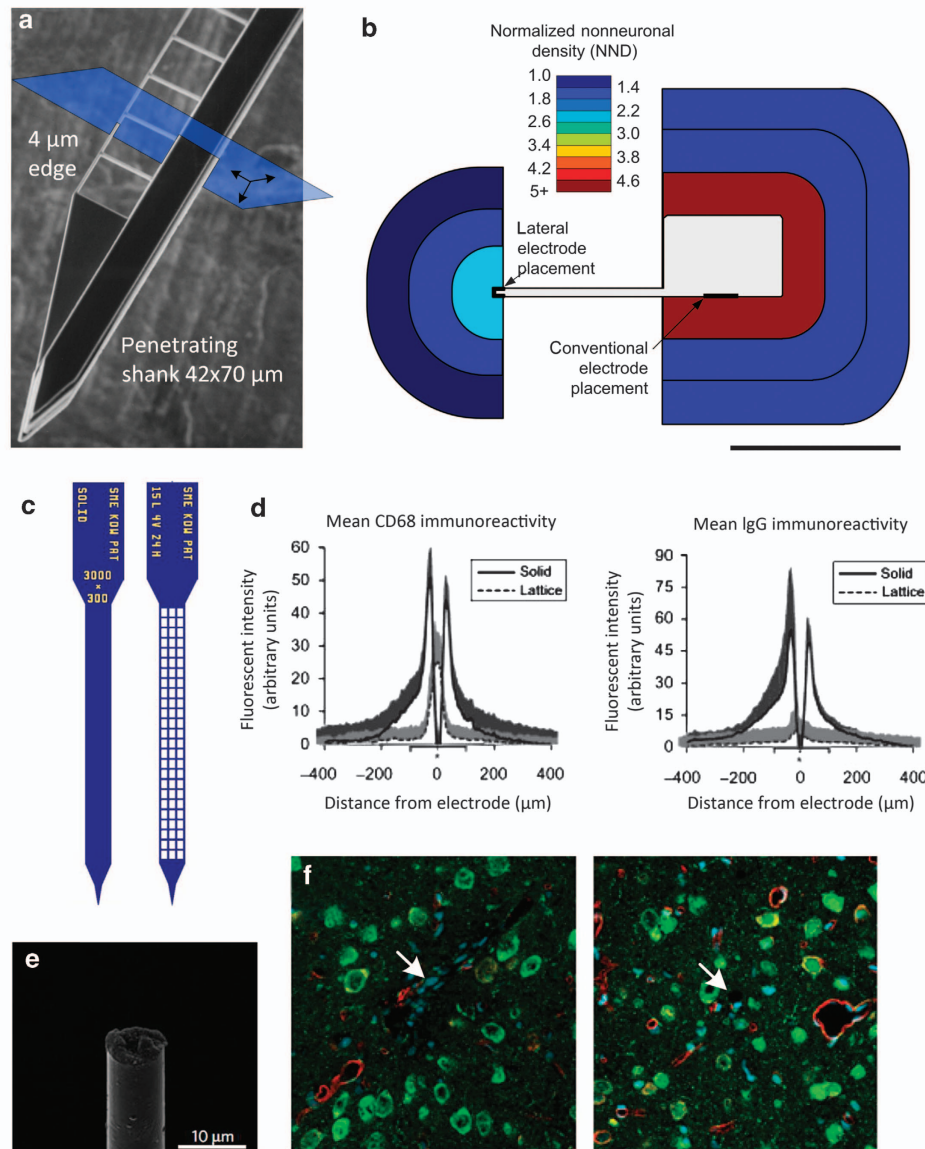
Figure 2 Seminal work supporting the hypothesis that the tissue response is a function of local device structure. (**a** and **b**) Tissue around the end of a thin polymer structure showed significant reduction in encapsulating cells (modified from Ref. 98). (**c** and **d**) Tissue response around solid and fine lattice structures showed significant reduction in reactive markers such as CD68 and IgG[99,104]. (**e** and **f**) Carbon fiber microthreads with an 8-μm diameter reduced tissue reactivity and improved neuron density of microthread[101]. IgG, immunoglobulin G.
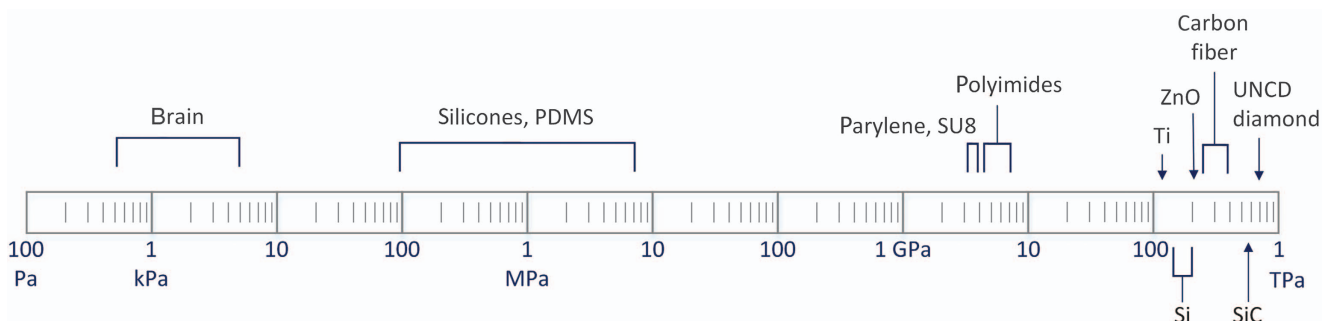

Figure 3 Log scale of elastic modulus for many substrates used in implantable arrays. Seminal research has covered inorganic substrates such as silicon[33], titanium[107], diamond[108], zinc oxide[109], and silicon carbide[110]. Studies on organic substrates have covered carbon fiber[101], parylene[111], SU-8[105,113], polyimide[114,115], and silicone[116].

under-utilized than PDMS are polyurethanes, polymers with urethane links (NH–(C = O)–O–), which may also prove important because their mechanical properties are highly tunable and their surfaces are readily functionalized[119,120].

Reducing the mechanical mismatch between a MEMS device and the extremely soft brain[121,122] (Figure 3) has been a focus of some research. The challenge is to insert a highly flexible substrate along a straight trajectory to a deep brain region. In addition, an insertion aid that has a sharp, rigid tip is necessary to pierce the dura or pia matter of the brain (Figure 1). One approach involves the creation of a biodegradable stiffener using silk over a thin parylene-C structure and shaping the silk with a microfabricated mold[123]. As indicated by Equation (2) (rectangular cantilever stiffness),

$$k = \frac{Ewt^3}{4\ell} \qquad (2)$$

lowering the Young's modulus E, the width w, and particularly the thickness t should greatly reduce tethering forces. Several groups have tried to quantify the local strain effects using finite element models[92,124]. Nonetheless, no research has clearly identified a threshold of relative stiffness that will mitigate the tissue response or, more importantly, enhance the recording quality. Silicones not only reduce the mechanical mismatch but achieve the greatest yield strain of all substrates used to date. Creating metal conductors that are resilient inside a stretchable substrate utilize wavy metal conductors[125,126], thin metals forming percolation networks[116,127], organic conductors[128,129], and stitched gold wires[130]. Further development of silicone or polyurethane substrates requires improving the feature resolution of the conductors and structures, validating the long-term adhesion and insulation of the conductors to the substrate, and engineering higher density packaging options.

An application in which flexibility and fracture toughness are absolute necessities is the electroencephalogram (ECoG). In this case, a microgrid is placed over the curved surface of the brain that requires close contact with the surface to maximize the recorded signal amplitudes. An early design used a polyimide substrate measuring 20 μm thick and had an electrode spacing of 1 mm (Ref. 68). Others have further improved the flexibility by developing a polyimide array measuring only 2.5-μm thick supported by biodegradable silk to aid in placement[131]. Most recently, the Buzsáki group developed the 'NeuroGrid,' a 4-μm-thick parylene-C ECoG array featuring low-impedance electrodes and a pitch of 30 μm to enable tetrode sorting techniques, resulting in the ability to record single-cell activity in both rats and humans[23] (Figure 1g). This latest development is particularly significant because it overturned the long-standing assumption that single-unit recordings were only possible with intracortical microelectrodes.

By far, the most successful material for intracortical extracellular neuroscience research has been silicon, which has led to at least four neural probe companies at the time of this writing. Some of most advanced silicon designs include double-sided, high-density arrays[29,102], three-dimensional arrangements[43], and integrated electronics[39,40,132]. Although the inherent brittleness of silicon is a concern for some clinical applications, its electrical, mechanical, and thermal properties offer the greatest design options and are supported by a wide range of commercial microfabrication tools. The large mechanical stiffness of silicon has been cited as a possible hindrance to long-term recording quality, but achieving thinner and finer structures would resolve this concern in many situations. Silicon devices can penetrate many brain types and depths. Unlike polymer arrays, silicon and other stiff materials have the ability to be moved on a microdrive during long-term recording and thereby maximizing the number of cells recorded in a session[106].

Other stiff materials include ultrananocrystalline diamond[108], SiC[110,133], and particularly carbon fiber materials[101,134]. These materials are all relatively new to field but have two significant advantages over silicon—a higher fracture toughness and a higher elastic modulus. These substrates may someday prove to be more reliable and achieve smaller dimensions in the hands of neuroscientists, but first manufacturing and handling limitations must be addressed.

Advanced electrodes

The electrode recording site is ultimately the interface where cellular activity is accessed and where some improvements must continue to be made. Sites are usually at least 10 μm in diameter, but the real tissue interface occurs at the scale of the electrical double-layer (Helmholtz layer), which makes all electrode technology from the EEG scale to the single-cell scale fundamentally a nanotechnology challenge. Several extensive reviews provide a historical perspective of this research space[135,136]. Electrical stimulating and recording electrode requirements share some similarities, but the electrochemical stability and current injection requirements of stimulation demand greater rigor in material selection and validation. Attention to charge-carrying capacity, charge balancing, voltage limits due to water hydrolysis, and long-term testing is required for function electrical stimulation, which continues to make important contributions to neuroscience[137].

Electrode requirements for recording have evolved as scientists have debated the optimum site impedance and size. Lempka et al. modeled the effect of electrode size on signal amplitude and showed that site diameters ranging from 7.5 to 20 μm produced nearly identical amplitudes; however, large pyramidal cells were assumed as current dipoles[138]. The results may be very different when recording near apical dendrites or smaller cell types. When site sizes > 20 μm can be used, thin-film materials such as Au, Pt, and Ir often show good performance. For tetrode sorting techniques discussed above, a pitch (diameter plus gap) as small as 20 μm is desirable. In these applications, thin-film Au, Pt, and Ir would all produce significant noise without additional steps to increase surface roughness. Research has demonstrated that electroplated Au[29], reactive sputtering of TiN[139], sputtered iridium[140], and activated iridium[139] all lower the electrode impedance and decrease the electrical noise. Modification of the electrode material or the deposition method is a well-proven means to lowering the impedance and therefore the thermal noise. This modification is also likely to lower susceptibility to electromagnetic interference[76,141].

New electrode alternatives continue to be developed and tested because past methods either do not provide sufficiently low noise or are unstable over time in vivo (or may provide insufficient charge storage capacity for electrical stimulation). Delamination and stability of the coating is a serious challenge. Causes include mechanical and chemical instabilities that are a function of the deposition method or due to non-reversible redox reactions. Furthermore, after implantation, the electrode will immediately biofoul and undergo electrochemical interactions. Over the last decade, conductive polymers, particularly poly(3,4-ethylenedioxythiophene) (PEDOT), have received much attention, outperforming thin-film metals in the first several weeks of use before biofouling and the foreign body response presumably reduce performance[142,143]. PEDOT has excellent charge injection capacity[144] and one of the lowest site impedances per unit area of any material. The two most common dopant molecules for PEDOT are polystyrene sulfonate (PSS) and, more recently, carbon nanotubes (CNT)[143]. Nevertheless, no electrode material has proven to monitor single neurons for years or even months without significant degradation in the signal-to-noise ratio; thus, more research on the electrode-tissue interface is certainly needed.

Regardless of which advanced material may solve this problem, the manufacturing method chosen is an important part of development. Some common electrode materials for brain research, for example, electroactive iridium, electroplated gold, and electrodeposited PEDOT, are deposited after the electrode array is in the final assembled state. This approach creates efficiency and uniformity challenges that could be better addressed at the wafer level, for example, batch electrodeposition. A cost-effective solution recently demonstrated is the use of a dry etchant to roughen thin-film gold at the wafer level[145], resulting in impedance values similar to those of PEDOT. Methods such as this may prove to be effective to neuroscientists and efficient to neurotechnologists.

STIMULATING BRAIN ACTIVITY
Introduction to optogenetics
Recording passively from local brain circuits is informative, but neuroscience can be much more effective at mapping a circuit by using controlled stimulation while monitoring cellular responses and their correlation to animal behavior. Over the past few decades, the electrical stimulation of the brain has provided tremendous insight into its functionality[146,147]. However, advanced neuroscience capable of studying cellular interactions in complex networks can be accelerated with selective activation or silencing of neurons of specific types. This feat cannot be achieved easily by electrical stimulation due to its lack of spatial resolution, non-specific stimulation, and the inability to silence neurons[148].

Optogenetics has begun to improve neuronal circuit analysis by introducing photosensitive proteins (opsins) into specific cell types such that these cells can respond to an optical stimulus with defined action potential patterns[8,149]. Using an appropriate wavelength to target a particular opsin(s), cell-type specificity can be achieved with well-controlled spatial and temporal resolution (on the order of milliseconds)[7]. For example, channelrhodopsin-2 (ChR2) and halorhodopsin can be co-expressed in the same cell types for the depolarization and hyperpolarization of this specific target using blue light (~473 nm) or yellow light (~590 nm), respectively[7,150–154]. This specific targeting allows for more sophisticated manipulations of neural activity and the testing of spike timing during specific neural computations and behaviors, but the sophistication is also a function of the light delivery tool itself. A major trend in optogenetic stimulation is the improvement of spatial selectivity because illuminating large volumes of tissue introduces a number of potential confounds to the experiment. There is the possibility of altering the threshold of excitation or creating

action potentials because of light absorption and heat[155] and the superposition of multiple spike waveforms on recording channels[156]. Furthermore, stimulating many neurons in synchrony is not a natural way to generate synthetic input[157]; therefore, we discuss several technological approaches that can address these limitations. Two-photon stimulation techniques offer the greatest spatial resolution[158] and a large field of stimulation, but because it is not capable of accessing deeper tissue structures and requires head-fixed experiments, there continues to be great interest in improving MEMS-based optical stimulation devices.

Early development of optogenetic tools
Despite recent rapid advances in optogenetics, supporting technologies for reliably delivering light to and record electrical signals from deep brain structures are not readily available. Early work involving in vivo optogenetics relied on the manual assembly of commercially available components such as microwires and optical fibers, which are not only bulky but can also experience large misalignments due to human error[9,159]. Since then, engineering efforts have gradually evolved towards MEMS technologies for miniaturization, high-density integration, and precise definition of the probe dimensions with lithographic resolution. For example, MEMS dielectric waveguides fabricated on silicon substrates for stimulating the brain at multiple locations with blue and red light have been reported[160]. However, no recording electrodes were integrated on these devices; therefore, they could not support both optical stimulation and electrophysiology. Stark et al.[9] reported a hybrid approach for manually assembling optical fibers onto MEMS recording probes. Coupled to laser diodes of various emission wavelengths, this device could excite and silence neural populations monitored by a high-density electrode array[161]. Nevertheless, the manual attachment (gluing) of fibers to each probe shank is very labor-intensive, resulting in potential misalignments and contamination of the recording sites by misplaced glue.

MEMS optical waveguide integrated probes
Advanced MEMS technologies can enable micron to sub-micron-scale features to be accurately defined using lithography. Planar architectures such as the 'Michigan style' probe shown in Figures 1e and f are particularly attractive for the integration of optics because of the versatility in depositing and patterning additional layers to form high-density optical and optoelectronic components.

Some of the first neural probes monolithically integrating both optical and electrical components are illustrated in Figures 4a–g.
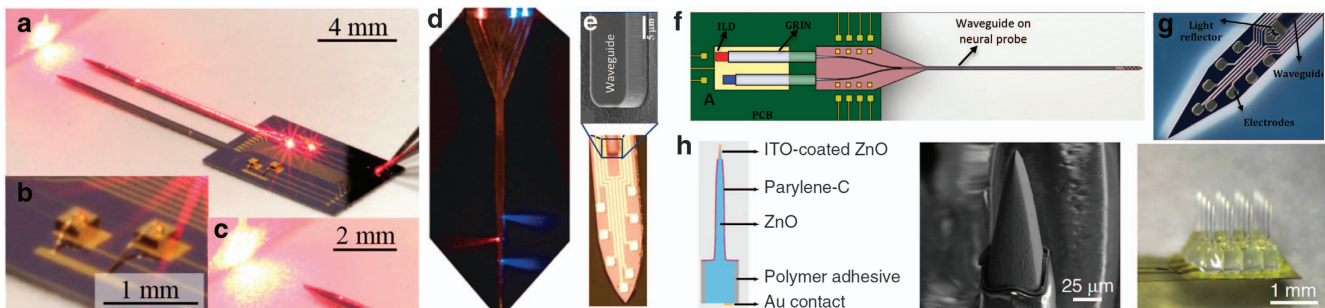

Figure 4 Example optoelectrodes with integrated waveguides: (a–c) Laser diode coupled waveguide probe demonstrating diode directly mounted on neural probe[165]; (d) a digital micromirror directing multi-color light into waveguides terminated with metal-coated corner mirrors[171]; (e) single waveguide on a silicon recording array[162]; (f and g) schematic of multi-color laser diodes coupled from a PCB using graded-index lenses and mixed on the neural probe and micrograph of an actual device[166]; and (h) a 4x4 ZnO array demonstrating a very similar form factor as the Utah array with the added capability of optical stimulation through the ZnO tine and ITO-coated tip[109].

In these devices, an optical waveguide is integrated onto the probe shank to deliver light from an externally coupled optical source to a stimulation site at the center of an integrated electrode array[162]. The waveguide can be made out of polymers such as SU-8 (Refs. 163,164) or dielectrics[162] and has a small rectangular light emission area on the order of $100\ \mu m^2$. The lithographically defined waveguide has a precisely positioned stimulation site relative to the recording sites to provide the spatial resolution necessary for circuit mapping (Figure 4e). The waveguide can also be freely configured to guide light through different paths[164] or to have multiple stimulation sites[160,163] for specific application needs (Figure 4d). The probe shank dimensions are defined with micron resolution using a double-sided DRIE process on an SOI wafer. Even a simple design having a single waveguide and eight electrode sites can demonstrate the utility of optogenetics from a high-density population such as the CA1 pyramidal layer in a rat by optically inducing single-unit activity from two cell types, which can be distinguished by the relative timing between the induced spikes and the light stimuli[162].

An important modification to the waveguide approach is eliminating the need for a tethered optical fiber because it can severely limit animal movement, especially when multiple fibers are used. A recent report demonstrated the feasibility of coupling a bare laser diode chip to an integrated waveguide[165]. The semiconductor light-emitting device requires only thin flexible cables for power, which is attractive for freely behaving animal experiments. Using unpackaged bare laser chips has the advantage of efficient coupling to waveguides with a similar numeric aperture (Figures 4a–c) and reaching optical intensities of up to 29.7 mW mm^{-2} using a red (650 nm) laser diode. Given the high cost of laser diodes and alignment and packaging, it may be useful to package the source at the PCB and either butt couple or focus the source into the probe. A recent example of this approach used commercially available gradient refractive index lenses to couple end-fire lasers[166,167] (Figures 4f and g). Another solution was demonstrated with a novel substrate material, zinc oxide, to form both the recording channel and waveguide in a form factor and fabrication method similar to the Utah array[109] (Figure 4h). Both the on-chip and on-PCB approaches will undoubtedly be useful, but as one scales the number of independent light sources or stimulating at higher duty cycles, the on-PCB approach may be the better choice, as evidenced by thermal modeling. In contrast, coupling an light-emitting diode (LED) to a waveguide is a fundamentally inefficient task due to the Lambertian emission profile of LEDs and the small area of minimally invasive waveguides.

The equations governing the basic design constraints of coupling a light source to a waveguide and then coupling the light into tissue are highly dependent on material and geometry. To briefly summarize, thin-film approaches allow engineers to maximize irradiance in the tissue using the equation

$$I = P_s \cdot \eta_{coupling} \cdot \eta_{scatter} \cdot \Phi_{geometry} \qquad (3)$$

where P_s is the optical power of the source, η is the coupling efficiency or scatter efficiency, and Φ is the function accounting for geometric spread as a function of depth, waveguide radius, and numerical aperture[168]. By careful selection of materials and the waveguide geometry, the optoelectrode can be chosen to match the refractive index at each optical interface to maximize coupling, but it is also desirable to maximize the numerical aperture of the waveguide to accept a wider angle of incoming light and to emit a wider angle at the output using Equation (4),

$$NA = n_0 \sin \theta_a = (n_{core}^2 - n_{clad}^2)^{1/2} \qquad (4)$$

where n_0 is the surrounding refractive index and θ_a is acceptance angle. These factors are also related to the index of the core and cladding. Furthermore, the maximum efficiency in source-coupled waveguide is given by Equation (5),

$$E_c = A_{WG} NA^2 / (A_{source} n_0^2) \qquad (5)$$

where A_{WG} is the cross-sectional area of the waveguide and A_{source} is the area producing light at the emitter. Even a small LED ($100 \times 100\ \mu m$) will have a source area, A_{source}, ~10 000 times larger than that of a typical laser diode. On the far side of the waveguide, light will enter the tissue, and the effects of geometric spreading and light scattering inside the tissue create some constraints on the volume of tissue that will be irradiated. The first is the spreading angle. Equation (4) can also be used to calculate the divergence angle of light in the tissue, but in that case $n_0 = n_{tissue}$. Unlike geometric spreading, scattering is a function of the wavelength of light[168]. Calculating the volume of excitable tissue also requires that some assumptions be made. First, one must estimate the irradiance threshold at which a neuron can be stimulated or silenced, which is a function of the opsin type, the consistency of expression in a cell, and local neuron orientation[9,169]. A second assumption must be made about the maximum irradiance allowed in tissue before heating[170] and cellular[155] changes occur. A Matlab tool for predicting the tissue irradiance and the heat generated using different spatial and temporal light input was provided by Stujenske et al.[170]. Despite these limitations, there is plenty of room for customizable illumination patterns given our control of numerical aperture, waveguide dimensions, and the addition of micromirrors[160,171] and diffusion elements. Photonic waveguides are commonly fabricated with micron dimensions, and thus, the number of independent light ports will increase rapidly, especially as the light sources are more efficiently packaged and coupled at the device backend.

MEMS LED integrated probes

An alternative to using a waveguide to transmit light from an external source to the probe tip is to integrate the light sources onto the probe tip directly. InGaN LEDs are attractive for optogenetic applications because the emission wavelength can be tailored for the activation of common opsins[172].

GaN-based LEDs are most commonly grown on sapphire or SiC substrates for minimal lattice mismatch at the GaN-substrate interface[173] because this structure enables efficient electron-to-photon conversion. Recently, LED arrays fabricated from a sapphire substrate have been demonstrated for optogenetics[174]. Thermal and optical characterization shows that blue LEDs can deliver enough optical power to activate ChR2 without overheating the tissue. However, no recording electrodes were integrated with these optical sources, and the probe shanks were not released from the sapphire wafer. The report demonstrates that the probe shanks can be patterned by laser dicing and that the substrate can be thinned mechanically; however, this approach may not achieve a needle-like probe body sufficient for fine features with minimal tissue damage.

To circumvent the difficulty in patterning conventional substrates such as sapphire, LEDs originally grown and patterned on sapphire can be transferred to another substrate by a laser lift-off technique. Figure 5a shows the assembly of several microfabricated LEDs at the tip of a flexible polymer platform for light generation precisely at the stimulation sites[175]. This approach is highly versatile, allowing for the integration of not only LEDs of different colors but also photodiodes and temperature sensors in a multi-layer structure to monitor the performance of the LEDs. Although the individual LEDs could be made relatively small ($50 \times 50\ \mu m$), the hybrid assembly resulted in a probe shank width of over 400 μm. Once implanted, the LEDs can be wirelessly controlled.
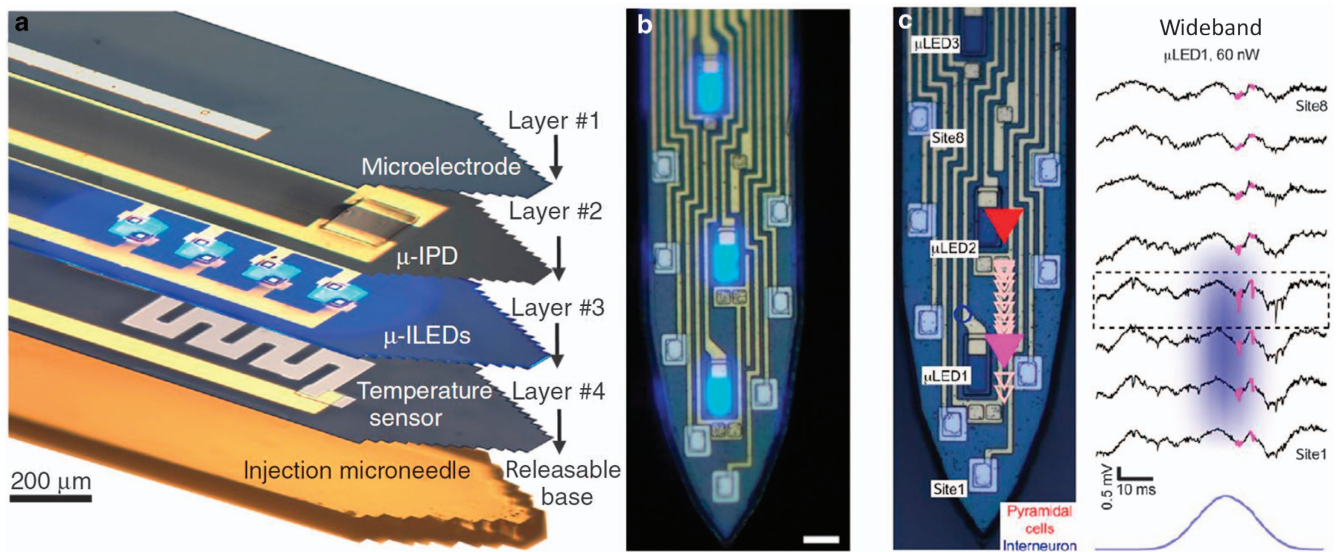
Figure 5 Fiberless optical stimulation using μLEDs. (**a**) GaN μLEDs grown on sapphire wafers and transferred onto a polymer substrate by laser-liftoff achieved 50 × 50 μm² μLEDs[175]. (**b**) First demonstration of monolithic integration of multiple GaN μLEDs on silicon neural probes and capable of a 50 μm pitch. Scale = 15 μm. (**c**) *In vivo* demonstration of same optoelectrode controlling pyramidal cells (PYR) in distinct parts of the CA1 pyramidal cell layer[176].

Our group's ongoing work on the monolithic integration of μLEDs and electrodes onto silicon probe shanks is highlighted in Figures 5b and c. This highly scalable approach allowed for 12 μLEDs and 32 electrodes to be integrated onto a four-shank probe, where each shank was only 70 μm wide[176]. The μLEDs and electrodes have been defined to have cellular dimensions, which can provide high spatial resolution for single-unit stimulation and recording in a highly populated brain region. The biggest challenge to any μLED approach is reducing μLED crosstalk, often called stimulation artifact. Addressing this challenge will require improved EMI immunity and better system integration at the backend.

We reviewed two broad approaches to fiberless optical stimulation: the use of an optical waveguide to transmit light from an external source and LEDs integrated next to the recording channels. The waveguide approach affords the ability to choose from commercial light sources, with many available wavelengths and output power levels available. Coupling into the waveguide is greatly improved with the use of advanced packaging tools such as a die bonder. Furthermore, the electromagnetic interference and heat generated by the light source are more easily managed given the greater distance from the susceptible recording channels. In contrast, the direct integration of light sources on the probe shank allows for highly efficient coupling into tissue and creates a stimulation zone well matched to the recording zone. The LED efficiency is closely associated with the semiconductor-to-substrate interface defect density. Thus, the light-emitting materials and substrate are constrained, limiting the available wavelengths and process compatibility. Obtaining a reasonable power efficiency is much more critical for this approach than for the waveguide approach because heat is generated near the cellular population of interest. Nevertheless, the LEDs can be scaled more effectively than the waveguides in terms of reducing their size and increasing their number, with the potential for highly confined stimulation at multiple locations. In addition, μLEDs consume less power than commercial laser diodes and therefore will be more easily powered wirelessly, which is ideal for behavioral animal experiments (assuming the cost is practical). Both approaches can offer advantages for particular optogenetic applications; however, significant engineering efforts are still

needed to achieve their full potential in neuroscience and possible clinical applications.

Fortunately, the field of nanophotonics has developed many approaches to integrating light sources and efficiently transmitting and modulating light. Optogenetics will benefit greatly from these rapid advances, and several groups have already provided evidence that light stimulation arrays are capable of matching the density of electrical recording technology. With greater effort in microsystem design, advanced packaging, and easy-to-use software interfacing, optoelectrode technologies will transition from being used in a few neuroscience laboratories to widespread use.

SCALABLE IMPLANTABLE MICROSYSTEMS

Current state-of-the-art electrical recording systems are still far from matching nature's scale in the central nervous system. The mouse brain has approximately one neuron in every 22 μm voxel[74], which only passive electrodes can match in 2D, but certainly not in 3D. Although electrical interfaces have been noticeably bad at achieving spatial scale, the resolution and breadth of their temporal domain continues to make this mode very attractive to neuroscientists. The average action potential is ~2 ms long and shows spiking (periodicity) at approximately 5 Hz, although this spiking could be in the range 0.5 and 500 Hz (Ref. 177). A 1 kHz bandwidth can capture most details of a cell, from the single neuron to population activity. Neuroscientists often prefer an ~0.1–10 kHz bandwidth with sub-microvolt analog-to-digital converter (ADC) resolution so that one may analyze the waveform shape itself. Even at a 10 kHz bandwidth, the digital clock speeds in a typical smartphone could sample ~100 000 electrode channels with excellent fidelity.

The scaling bottleneck continues to be the spatial limits of the analog front-ends and the electrode array itself. The first significant limitation of recording systems is the sheer number of interconnects required. When the shank width increases beyond 50–80 μm, there is a noticeable loss of neural signals, thus making this range of widths a widely accepted upper limit. However, as few as 128 channels on one narrow shank pushes the resolution toward expensive manufacturing options such as e-beam or deep ultraviolet lithography. Even if resources were
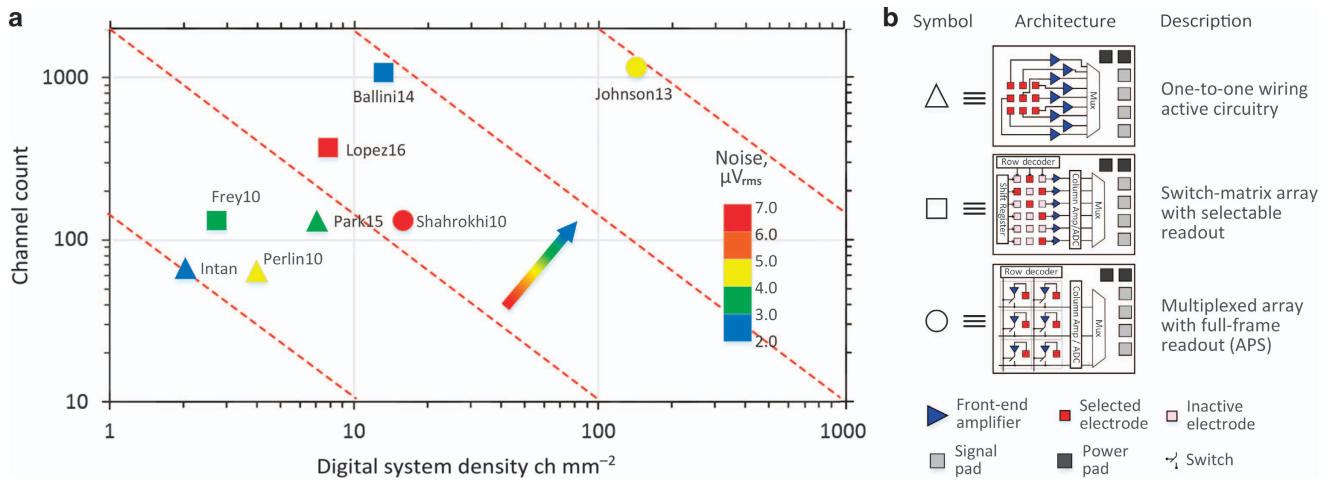
Figure 6 Scalability of leading high-density recording systems having integrated digital output. (**a**) Channel count versus density for three different architectures. Color indicates the input-referred noise (μVrms). Actual channel count was significantly lower compared with the number of available recording sites for the switch-matrix architecture (□). The arrow indicates the direction and color of advancing microsystems. (**b**) Legend for inset A showing three common architectures discussed in recent work. Table 1 draws further comparison.

unlimited and e-beam lithography, for example, could be used to pattern the interconnects, the next bottleneck becomes the bonding pad interface, whether it be a cable, PCB, or an ASIC. Recently, one group demonstrated the feasibility of e-beam interconnects resulting in a 1000 microelectrode array, but the structure was still limited by having a very large silicon backend and PCB[178]. We believe the recent advancements in packaging and mixed-mode circuit design are creating a unique opportunity that will accelerate efforts to address scale. We explore some of the latest research that is addressing these limitations, including alternative analog front-end architectures and packaging.

High-density active recording
Because the vast majority of neurons we have access to are just above the noise floor (~5–20 μV), the strategy of integrating on-chip amplifiers is an attractive one. Low-noise amplifiers (LNAs) on the same substrate as the electrode array (or packaged very close to it) will in theory reduce the load capacitance and attenuation of the biological signal. Short leads also reduce inter-channel crosstalk and become less susceptible to electromagnetic interference. Ideally, the analog front-end density should match that of the electrode array density. Furthermore, if the area spanned by the electrodes could even include the ADC and data serialization circuitry, then what would limit its scalability? If this challenging proposition could be achieved, then the field would have an unprecedented active system—one that is truly expandable and not limited to choosing only a few regions. We discuss recent analog-to-digital systems that have made impressive gains in area efficiency and some of the performance tradeoffs that should be addressed.

A comparison of the highest-density and highest-performing systems is shown in Figure 6. Inclusion in this comparison requires that the ASIC integrate the digital convertors with the analog-front end and be capable of wideband recording. Although MEA amplifiers and in vivo amplifier ASICs have historically been considered different device types, we wanted to directly compare the best area efficiency from each camp. It should also be noted that the lines between in vivo and in vitro are blurring because the ASIC can become the probe. A large project undertaken by researchers at HHMI and Imec has recently resulted in an implantable ASIC with 966 selectable channels by post-processing CMOS

circuits using a silicon-on-insulator 130 nm process[179]. ASICs may also be further post-processed into flexible arrays, using deep reactive ion etching, that stop on several pre-defined metal etch stops to leave only islands of interconnected electrodes and amplifiers[180]. Other ASICs we include (Figure 6, Table 1) are designed for in vivo use and packaged on the backend of the system (intantech.com, Park15 (Ref. 181), and Perlin10 (Ref. 182)). This contrast also allows for the comparison of three different architectures (Figure 6b): (i) one-to-one mapping of electrode to a high-gain LNA, (ii) multiplexed array with a switch matrix to allow site-selective multiplexing, and (iii) a multiplexed array with full-frame readout similar to an active pixel sensor (APS) imager.

Table 1 compares many of the performance metrics of each example as well. It is also critical to note that the many performance metrics can shift in weight based on the application. It can be argued that the emphasis on system density (Figure 6) should not overlook the other metrics. The common-mode rejection ratio, for example, is an important predictor of noise immunity when using a system in awake behaving animals. Obviously, a wireless or battery-powered system places a premium on low power; therefore, the advantages and disadvantage of each approach should be considered in context. Table 1 shows a variety of tradeoffs. The commercial Intan system is currently the lowest-cost solution and exhibits excellent noise performance, but at some cost to size and power. Park15 has been optimized for the combination of low power, high resolution, and moderate density. Lopez16 (Ref. 179) successfully implemented a channel selection switched matrix as the neural probe itself with many competitive metrics. Ballini14 (Ref. 183) and Johnson13 (Ref. 184) achieved the two highest densities with competitive input-referred noise values, but these devices were tested over a higher frequency band, limiting a proper comparison. Nonetheless, the magnitude of the system density suggests that future systems may choose scale over the slight limitation of a smaller bandwidth tuned only for single-unit activity (for example, 300–5000 Hz).

Regarding the noise performance of the various systems, the noise amplitude is somewhat crude because it is not uniformly tested and is a function of both the bandwidth and the actual band. For CMOS devices in particular, flicker noise or 1/f noise is the dominant source at low frequencies (corner frequency is typically 500–10 000 Hz) for small transistors. Input referred noise

Table 1 Performance comparison of leading system architectures

	Perlin10	Intan	Park15	Frey10	Ballini14	Lopez16	Shahrokhi10	Johnson13
Architecture, Figure 6b	One-to-one (Δ)			Selectable (□)			Active pixel (○)	
Sampling rate, kHz	16	30	25	20	20	30	14	20
Input noise, µVrms	4.8	2.4	3.3	3.0	2.4	6.4	6.1	4.3
Bandwidth, Hz	10–10k	0.1–10k	0.4–11k	1–100k	300–10k	0.3–10k	10–5k	20–50k
Total power/Ch, µW	—	830	19	1107	73	49	19	—
CMRR, dB	—	—	60	—	72	>60	60	21 (66)[a]
ENOB/resolution	—/8	—/16	10.9/1[b]	—/8	—/10	—/10	6.2/8	8.2/10
No. of Ch. availability	64	64	128	122	1024	384	128	1120
No. of electrodes	64	64	128	11 011	26 400	966	128	1120
Tech node, nm	500	—	180	600	350	130	350	180
Reference	182	[c]	181	188	183	179	189	184

Abbreviations: Ch, channel; Tech, technology. [a]CMRR measured to be 21 dB, but after principal component analysis was performed, 66 dB was achieved. [b]ADC oversampled 32X. [c]www.intantech.com.

can be skewed by a limited bandwidth and particularly by a large high-pass frequency such as 20 Hz (Table 1). A few important points are worth noting in the model for the flicker noise voltage spectrum S^2:

$$S_{1/f}^2(f) = \frac{K_f}{C_{ox}A}\frac{1}{f^a} \qquad (5)$$

where K_f is a technology feature size and is a foundry-specific value, C_{ox} is the gate oxide capacitance and A is the area of the gate. The exponent a is another empirically measured value and determines the slope of the low-frequency response (typically close to 0.9 for NMOS and 1.1 for PMOS)[185,186]. A large a will attenuate the noise faster with respect to frequency and thus is desirable. C_{ox} is the normalized capacitance, which generally increases with decreasing feature size but will vary depending on the oxide thickness of a given process. Although most LNA circuit designers tend to choose large process nodes (180–600 nm, Table 1), there has been a slow but steady trend toward advanced nodes. One group demonstrated very low noise in a 65 nm node that also had a small amplifier area[187] of 0.013 mm^2, although with only two channels. Circuit designers should also pay close attention to the process-defined values of K, C_{ox}, and a, which will help reduce noise. Even if transistors must be made much larger than required by the technology node for an equivalent noise floor, the digital circuit design in particular will benefit from the higher density and lower power of a smaller node. Future solutions may also employ the mixing of processes by vertical integration or by special processes such as graphene or SiGe BiCMOS. SiGe BiCMOS can employ low-noise bipolar transistors in the front-end and high-resolution low-power CMOS in the digital domain.

Given these size-performance constraints related to flicker and thermal noise, the strategy employed by the switch matrix architectures (Figure 6) is to separate amplification stages such that a smaller circuit is near the electrode. The electrode stage amplifier is switched into a column readout amplifier, which generally is a programmable gain amplifier (PGA) connected to an ADC. It has been a precept by many that having a dedicated LNA, PGA, and ADC per channel would provide the lowest noise design, but the noise performance of a few switched-matrix MEAs has become good enough that the density advantages may now be attractive for *in vivo* use. To date, very few integrated microsystems have been tested in animals; thus, further *in vivo* validation is needed to assess biological noise and motion artifact noise. The switched matrix design also reduces the number of interconnects leading to the array itself from (row count × column count) to only slightly more than (row count + column count). But

the selectable[179,183,188] and the active pixel architectures[184,189], have important differences between them.

Using a switched matrix architecture with selectable electrodes (Table 1) is an effective way to reduce power in a circuit design. One can switch the data stream to regions of high activity and ignore quiescent regions. However, an important limitation of this architecture can be illustrated in the context of a clinical application such as a brain-machine interface versus brain mapping. In the former, the clinician can scan for *a priori* features in the neural data, but in the latter, almost nothing is *a priori*. Once a putative neuron signal is found, it is especially important to look across the entire array in search of network effects—activity occurring immediately before and after the action potential to help determine coherence, phase, and ideally, network connections. Selective spike detection as a means of data compression is a challenging and risky proposition for circuit mapping because when one threshold event occurs (a putative neuron), one must simultaneously analyze many or all of the channels on the array or risk losing valuable data. For a high-density array, there will be a good probability of one neuron firing at almost any moment in time, and thus, sampling sporadically is only useful when much is already known. Therefore, high-density full-frame readout schemes such as the 'active pixel' approach will ultimately be most attractive to systems neuroscientists.

Packaging developments

The packaging requirements for implantable and wearable neurotechnology are generally to protect the tissue from heat, to protect the electronics from the ingress of water and ions, and to minimize the device dimensions while presenting a user-friendly form factor. A variety of solutions to these problems have already been pioneered using microfabrication methods to package gyroscopes, infrared sensors, and resonators in very difficult non-biological environments. These applications require atmospheric, thermal, and mechanical isolation and thus provide neurotechnologists with many useful strategies. Similarly, advancements in the vertical stacking of ICs, also known as system-in-package, are providing new methods of packaging to address the needs of combining dissimilar technologies such as MEMS, CMOS ASICs, and memory. Several reviews such as (Refs. 190 and 191) cover a range of creative methods for achieving ultrahigh-density packaging. We will discuss recent work that has borrowed from these two broader packaging developments and have been applied to neurotechnology.

Commercially available recording and stimulating technologies rely on relatively low-density methods; hence, the typical backend of a silicon neural probe consumes the largest area on a given mask set. Wire bonding is the most common method for

connecting to a silicon device, and typical bonding pad pitches are 100–150 µm. For polymer substrates, MicroFlex interconnection (a form of ball bumping) offers an alternative to wire bonding but has a similar pitch[192]. Certain high-end consumer products are capable of 40–50 µm pitch, and state-of-the-art packaging research has demonstrated 10 µm pitch using microbumps and flip chip bonding[193]. Unfortunately, these approaches also require greater investment in packaging tools such as die bonders with highly precise thermocompression and alignment capabilities. Finally, the testing tools that ensure reliability will also become more costly with increasing scales and finer features.

Nonetheless, research continues to demonstrate promising solutions. In one example of neural probe-to-ASIC integration, Xie et al. improved the encapsulation performance of a wireless microsystem flip-chip mounted on a Utah-style array. Al_2O_3 was deposited by atomic layer deposition on both the passive recording array and the integrated backend to significantly extend the lifetime of both compared with the use of parylene-C alone[194]. In another example, Perlin et al. demonstrated 3D stacking of high-density planar arrays that were interconnected on a common platform through the novel use of tabs with a pitch of 40 µm (Ref. 182; Figure 1j). Consumer electronics have also created a demand for the stacking of silicon devices. Vertical feedthroughs in an IC die allow the circuit to be stacked on other ICs or on an interposer with multiple ICs in parallel (also known as 2.5D technology). This technology could become a cost effective way to integrate neural probes and front-end amplifiers. Through-silicon-vias (TSVs) have now matured to the point that TSVs within interposers or stacked ICs have demonstrated high yield by a number of vendors. TSVs can also be built into the exterior of a sensor capsule[195], similar to the way feedthroughs are built into medical devices. MEMS-based solutions for feedthroughs and hermetic capsules reduce the volume of a microsystem by several orders of magnitude compared with conventional titanium housings with ceramic feedthroughs. Furthermore, wafer-level packaging of sensor arrays and vertical enclosures have been demonstrated using a variety of low-temperature eutectic bonds[196] and thus also have the potential to be cost-effective and compatible with many materials.

Packaging is a significant roadblock to the implementation and commercialization of high-density microsystem tools for neuroscience. The field will continue to witness both monolithic and hybrid solutions in the coming years. Arguably, monolithic integration greatly simplifies the packaging challenge, but as the substrate materials continue to vary and new modalities arise, the field will undoubtedly benefit from the ongoing advancements in heterogeneous vertical stacking. It is not difficult to imagine a day in the near future when vertical IC/MEMS integration is as simple as wire bonding is today. When this happens, we envision that the number of recording and stimulation channels on current ASICs will not necessarily increase, but instead, technologists will modularly package them in parallel on sensor and actuator arrays. In other words, the typical path forward is to move the arrow on the channel count versus density plot (Figure 6) directly orthogonal to the figure of merit, but there might be an advantage if chipsets feature a low channel count and therefore are easily distributed throughout the system. CPU speed and transistor count, by analogy, are no longer steadily increasing; instead, computer makers have relied on parallel processing. With this in mind, hybrid packaging approaches appear to be a practical solution for addressing the need for scalability while acknowledging that applications such as brain mapping and medical devices are inherently small-volume.

FUTURE TECHNOLOGIES FOR NEUROSCIENCE RESEARCH
Since 1990, over one thousand neuroscience and neural prostheses studies have used silicon-based neural probes for monitoring brain activity, and an increasing number using both light stimulation and recording arrays in tandem are being published. Although these advancements are impactful, both neuroscientists and technologists agree that our current rate of development is insufficient to expect major breakthroughs in neuroscience without improved scale, density, and specificity. The goal of reverse engineering even a basic brain function, such as memory or learning, may be many years away given that our tools are still very crude compared with the systems under study. There are no trivial solutions because sensors, actuators, ASICs, and packaging must all progress in step if practical solutions are to become readily available to the larger neuroscience community. The field has recently witnessed an influx of new ideas and researchers with continued government and foundation investment anticipated. We can expect nascent technologies to become increasingly relevant and disruptive.

Optical methods of stimulating and monitoring neural activity have already become an important complement to electrical methods[197]. Future neuroscience discovery will undoubtedly rely on a novel combination of sensing and actuating modalities, but which will be most effective at revealing neuronal cell types and circuit function? Neurochemical sensing and control is arguably the most promising modality yet to achieve scale. Importantly, multimodal methods are needed to combine intracellular monitoring, such as monitoring protein or metabolic changes, with our current extracellular techniques. Although studying the electrical response of a cell in the context of behavior has been important, some experiments will additionally require monitoring intracellular changes, for example, RNA and protein changes[198], if we are to answer that most basic question: What makes any one neuron fire or not fire? This vision, we believe, will require long-term effort by MEMS and microsystems engineers working closely with neuroscientists. With further interest and investment, we expect the coming decade to see significant breakthroughs in our understanding of brain function and disease-related dysfunction.

COMPETING INTERESTS
FW is the VP of Product Development of Diagnostic Biochips, Inc., a for-profit manufacturer of neurotechnology. The remaining authors declare no conflicts of interest.

REFERENCES
1 Allen PG, Collins FS. Toward the final frontier: The human brain. Wall Street Journal 2013.
2 Azevedo FAC, Carvalho LRB, Grinberg LT et al. Equal numbers of neuronal and nonneuronal cells make the human brain an isometrically scaled up primate brain. Journal of Comparitive Neurology 2009; 513: 532–541.
3 Buzsáki G. Neural syntax: Cell assemblies, synapsembles, and readers. Neuron 2010; 68: 362–385.
4 Roux L, Stark E, Sjulson L et al. In vivo optogenetic identification and manipulation of GABAergic interneuron subtypes. Current Opinions in Neurobiology 2014; 26C: 88–95.
5 Fishell G, Heintz N. The neuron identity problem: Form meets function. Neuron 2013; 80: 602–612.
6 Alivisatos AP, Andrews AM, Boyden ES et al. Nanotools for neuroscience and brain activity mapping. ACS Nano 2013; 7: 1850–1866.
7 Boyden ES, Zhang F, Bamberg E et al. Millisecond-timescale, genetically targeted optical control of neural activity. Nature Neuroscience 2005; 8: 1263–1268.

8 Yizhar O, Fenno LE, Davidson TJ *et al.* Optogenetics in neural systems. *Neuron* 2011; **71**: 9–34.

9 Stark E, Koos T, Buzsáki G. Diode probes for spatiotemporal optical control of multiple neurons in freely moving animals. *Journal of Neurophysiology* 2012; **108**: 349–363.

10 Chuong AS, Miri ML, Busskamp V *et al.* Noninvasive optical inhibition with a red-shifted microbial rhodopsin. *Nature Neuroscience* 2014; **17**: 1123–1129.

11 Berndt A, Lee SY, Ramakrishnan C *et al.* Structure-guided transformation of channelrhodopsin into a light-activated chloride channel. *Science* 2014; **344**: 420–424.

12 Klapoetke NC, Murata Y, Kim SS *et al.* Independent optical excitation of distinct neural populations. *Nature Methods* 2014; **11**: 338–346.

13 Amatrudo JM, Olson JP, Agarwal HK *et al.* Caged compounds for multichromic optical interrogation of neural systems. *European Journal of Neuroscience* 2015; **41**: 5–16.

14 Ferguson SM, Neumaier JF. Grateful DREADDs: Engineered receptors reveal how neural circuits regulate behavior. *Neuropsychopharmacology* 2012; **37**: 296.

15 Zhu H, Roth BL. Silencing synapses with DREADDs. *Neuron* 2014; **82**: 723–725.

16 Dua T, Janca A, Kale R *et al.* Neurological disorders affect millions globally: WHO report 2006; Available at www.who.int.

17 Merolla PA, Arthur JV, Alvarez-Icaza R *et al.* A million spiking-neuron integrated circuit with a scalable communication network and interface. *Science* 2014; **345**: 668–673.

18 Lu W. Memristors: Going active. *Nature Materials* 2013; **12**: 93–94.

19 Verkhratsky A, Parpura V. History of electrophysiology and the patch clamp. In: Patch-Clamp Methods and Protocols. Springer Science+Business Media New York, 2014; 1–19.

20 Hodgkin AL, Huxley AF, Katz B. Measurement of current-voltage relations in the membrane of the giant axon of Loligo. *Journal of Physiology* 1952; **116**: 424.

21 Harvey CD, Collman F, Dombeck DA *et al.* Intracellular dynamics of hippocampal place cells during virtual navigation. *Nature* 2009; **461**: 941–946.

22 Gray CM, Maldonado PE, Wilson M *et al.* Tetrodes markedly improve the reliability and yield of multiple single-unit isolation from multi-unit recordings in cat striate cortex. *Journal of Neuroscience Methods* 1995; **63**: 43–54.

23 Khodagholy D, Gelinas JN, Thesen T *et al.* NeuroGrid: recording action potentials from the surface of the brain. *Nature Neuroscience* 2015; **18**: 310–315.

24 Buzsáki G. Large-scale recording of neuronal ensembles. *Nature Neuroscience* 2004; **7**: 446–451.

25 Hubel DH. Tungsten microelectrode for recording from single units. *Science* 1957; **125**: 549–550.

26 Steenland HW, McNaughton BL. Techniques for large-scale multiunit recording. In: Analysis and Modeling of Coordinated Multi-neuronal Activity. Springer Science+Business Media New York, 2015; 3–39.

27 McNaughton BL, O'Keefe J, Barnes CA. The stereotrode: A new technique for simultaneous isolation of several single units in the central nervous system from multiple unit records. *Journal of Neuroscience Methods* 1983; **8**: 391–397.

28 Moffitt MA, McIntyre CC. Model-based analysis of cortical recording with silicon microelectrodes. *Clinical Neurophysiology* 2005; **116**: 2240–2250.

29 Du J, Roukes ML, Masmanidis SC. Dual-side and three-dimensional microelectrode arrays fabricated from ultra-thin silicon substrates. *Journal of Micromechanics and Microengineering* 2009; **19**: 75008.

30 Swindale NV, Spacek MA. Spike sorting for polytrodes: A divide and conquer approach. *Frontiers in Systems Neuroscience* 2014; **8**: 6.

31 Blanche TJ, Spacek MA, Hetke JF *et al.* Polytrodes: high-density silicon electrode arrays for large-scale multiunit recording. *Journal of Neurophysiology* 2005; **93**: 2987–3000.

32 Ecker AS, Berens P, Keliris GA *et al.* Decorrelated neuronal firing in cortical microcircuits. *Science* 2010; **327**: 584–587.

33 Wise KD, Angell JB, Starr A. An integrated-circuit approach to extracellular microelectrodes. *IEEE Transactions on Biomedical Engineering* 1970; **BME-17**: 238–247.

34 Wise KD, Angell JB. A low-capacitance multielectrode probe for use in extracellular neurophysiology. *IEEE Transactions on Biomedical Engineering* 1975; **BME-22**: 212–219.

35 Najafi K, Wise KD, Mochizuki T. A high-yield IC-compatible multichannel recording array. *IEEE Transactions on Electron Devices* 1985; **32**: 1206–1211.

36 Najafi K, Wise KD. An implantable multielectrode array with on-chip signal processing. *IEEE Journal of Solid State Circuits* 1986; **21**: 1035–1044.

37 BeMent SL, Wise KD, Anderson DJ *et al.* Solid-state electrodes for multichannel multiplexed intracortical neuronal recording. *IEEE Transactions on Biomedical Engineering* 1986; **BME-33**: 230–241.

38 Hetke JF, Lund JL, Najafi K *et al.* Silicon ribbon cables for chronically implantable microelectrode arrays. *IEEE Transactions on Biomedical Engineering* 1994; **41**: 314–321.

39 Sodagar AM, Perlin GE, Yao Y *et al.* An implantable 64-channel wireless microsystem for single-unit neural recording. *IEEE Journal of Solid State Circuits* 2009; **44**: 2591–2604.

40 Lopez CM, Andrei A, Mitra S *et al.* An implantable 455-active-electrode 52-channel CMOS neural probe. *IEEE Journal of Solid State Circuits* 2014; **49**: 248–261.

41 Bhatti PT, Wise KD. A 32-site 4-channel high-density electrode array for a cochlear prosthesis. *IEEE Journal of Solid State Circuits* 2006; **41**: 2965–2973.

42 Johnson AC, Wise KD. An active thin-film cochlear electrode array with monolithic backing and curl. *Journal of Microelectromechanical Systems* 2014; **23**: 428–437.

43 Merriam ME, Srivannavit O, Gulari MN *et al.* A three-dimensional 64-site folded electrode array using planar fabrication. *Journal of Microrlectrochemical Systems* 2011; **20**: 594–600.

44 Yao Y, Gulari MN, Wiler JA *et al.* A microassembled low-profile three-dimensional microelectrode array for neural prosthesis applications. *Journal of Microrlectrochemical Systems* 2007; **16**: 977–988.

45 Ruther P, Aarts A, Frey O *et al.* The NeuroProbes project—multifunctional probe arrays for neural recording and stimulation. *Biomedical Technology* 2008; **53**: 238–240.

46 Norlin P, Kindlundh M, Mouroux A *et al.* A 32-site neural recording probe fabricated by DRIE of SOI substrates. *Journal of Micromechanics and Microengineering* 2002; **12**: 414.

47 Cheung KC, Djupsund K, Dan Y *et al.* Implantable multichannel electrode array based on SOI technology. *Journal of Microrlectrochemical Systems* 2003; **12**: 179–184.

48 Jones KE, Campbell PK, Normann RA. A glass/silicon composite intracortical electrode array. *Annals of Biomedical Engineering* 1992; **20**: 423–437.

49 Nordhausen CT, Rousche PJ, Normann RA. Optimizing recording capabilities of the Utah intracortical electrode array. *Brain Research* 1994; **637**: 27–36.

50 Rousche PJ, Normann RA. Chronic intracortical microstimulation (ICMS) of cat sensory cortex using the Utah Intracortical Electrode Array. *IEEE Transactions on Rehabilitation Engineering* 1999; **7**: 56–68.

51 Barrese JC, Rao N, Paroo K *et al.* Failure mode analysis of silicon-based intracortical microelectrode arrays in non-human primates. *Journal of Neural Engineering* 2013; **10**: 66014.

52 Santhanam G, Linderman MD, Gilja V *et al.* HermesB: a continuous neural recording system for freely behaving primates. *IEEE Transactons on Bio-medical Engineering* 2007; **54**: 2037–2050.

53 Linderman MD, Gilja V, Santhanam G *et al.* Neural recording stability of chronic electrode arrays in freely behaving primates. 2006 International Conference of the IEEE Engineering in Medicine and Biology Society (EMBS'06); 30 Aug–3 Sep 2006; New York, NY, USA; 2006: 4387–4391.

54 Truccolo W, Hochberg LR, Donoghue JP. Collective dynamics in human and monkey sensorimotor cortex: Predicting single neuron spikes. *Nature Neuroscience* 2009; **13**: 105–111.

55 Vogel J, Haddadin S, Simeral JD *et al.* Continuous control of the DLR light-weight robot III by a human with tetraplegia using the BrainGate2 neural interface system. In: Experimental Robotics. Springer International Publishing AG, Part of Springer Science+Business Media, 2014: 125–136.

56 Chadwick EK, Blana D, Simeral JD *et al.* Continuous neuronal ensemble control of simulated arm reaching by a human with tetraplegia. *Journal of Neural Engineering* 2011; **8**: 34003.

57 Hochberg LR, Bacher D, Jarosiewicz B *et al.* Reach and grasp by people with tetraplegia using a neurally controlled robotic arm. *Nature* 2012; **485**: 372–375.

58 Miranda H, Gilja V, Chestek CA *et al.* HermesD: A high-rate long-range wireless transmission system for simultaneous multichannel neural recording applications. *IEEE Transactions on Biomedical Circuits and Systems* 2010; **4**: 181–191.

59 Borton DA, Yin M, Aceros J *et al.* An implantable wireless neural interface for recording cortical circuit dynamics in moving primates. *Journal of Neural Engineering* 2013; **10**: 26010.

60 Yin M, Borton DA, Komar J *et al.* Wireless neurosensor for full-spectrum electrophysiology recordings during free behavior. *Neuron* 2014; **84**: 1170–1182.

61 Obien MEJ, Deligkaris K, Bullmann T *et al.* Revealing neuronal function through microelectrode array recordings. *Frontiers in Neuroscience* 2014; **8**: 423.

62 Hierlemann A, Frey U, Hafizovic S *et al.* Growing cells atop microelectronic chips: Interfacing electrogenic cells *in vitro* with CMOS-based microelectrode arrays. *Proceedings of the IEEE* 2011; **99**: 252–284.

63 Fromherz P. Electrical interfacing of nerve cells and semiconductor chips. *ChemPhysChem* 2002; **3**: 276–284.

64 Liu J, Wen J, Zhang Z *et al.* Voyage inside the cell: Microsystems and nanoengineering for intracellular measurement and manipulation. *Microsystems & Nanoengineering* 2015; **1**: 1–15.

65 Xie C, Lin Z, Hanson L *et al.* Intracellular recording of action potentials by nanopillar electroporation. *Nature Nanotechnology* 2012; **7**: 185–190.

66 Yang L, Li Y, Fang Y. Nanodevices for cellular interfaces and electrophysiological recording. *Advanced Materials* 2013; **25**: 3881–3887.

67 Rubehn B, Bosman C, Oostenveld R *et al.* A MEMS-based flexible multichannel ECoG-electrode array. *Journal of Neural Engineering* 2009; **6**: 36003.

68 Kim J, Wilson JA, Williams JC. A cortical recording platform utilizing μECoG electrode arrays. 2007 International Conference of the IEEE Engineering in Medicine and Biology Society (EMBS 2007); 22–26 Aug 2007; Lyon, France; 2007: 5353–5357.

69 Acar ZA, Acar CE, Makeig S. Simultaneous head tissue conductivity and EEG source location estimation. *Neuroimage* 2016; **124**: 168–180.

70 McDowell K, Lin C-T, Oie KS *et al*. Real-world neuroimaging technologies. *IEEE Access* 2013; **1**: 131–149.

71 Forvi E, Bedoni M, Carabalona R *et al*. Preliminary technological assessment of microneedles-based dry electrodes for biopotential monitoring in clinical examinations. *Sensors and Actuators A*: *Physical* 2012; **180**: 177–186.

72 Stevenson I. Tracking advances in neural recording. Available at http://stevenson.lab.uconn.edu/scaling/ (accessed 10 Apr 2016).

73 Stevenson IH, Kording KP. How advances in neural recording affect data analysis. *Nature Neuroscience* 2011; **14**: 139–142.

74 Marblestone AH, Zamft BM, Maguire YG *et al*. Physical principles for scalable neural recording. *Frontiers in Computational Neuroscience* 2013; **7**: 137.

75 Buzsáki G, Draguhn A. Neuronal oscillations in cortical networks. *Science* 2004; **304**: 1926–1929.

76 Loeb GE, Peck RA, Martyniuk J. Toward the ultimate metal microelectrode. *Journal of Neuroscience Methods* 1995; **63**: 175–183.

77 Robinson DA. The electrical properties of metal microelectrodes. *Proceedings of the IEEE* 1968; **56**: 1065–1071.

78 Harris KD, Henze DA, Csicsvari J *et al*. Accuracy of tetrode spike separation as determined by simultaneous intracellular and extracellular measurements. *Journal of Neurophysiology* 2000; **84**: 401–414.

79 Delescluse M, Pouzat C. Efficient spike-sorting of multi-state neurons using inter-spike intervals information. *Journal of Neuroscience Methods* 2006; **150**: 16–29.

80 Einevoll GT, Franke F, Hagen E *et al*. Towards reliable spike-train recordings from thousands of neurons with multielectrodes. *Current Opinions in Neurobiology* 2012; **22**: 11–17.

81 Rossant C, Harris KD. Semi-automatic spike sorting with high-count channel probes. *BMC Neuroscience* 2013; **14**: 1.

82 Rossant C, Kadir SN, Goodman DFM *et al*. Spike sorting for large, dense electrode arrays. *Nature Neuroscience* 2016; **19**: 634–641.

83 Tsien JZ, Li M, Osan R *et al*. On brain activity mapping: insights and lessons from Brain Decoding Project to map memory patterns in the hippocampus. *Science China Life Science* 2013; **56**: 767–779.

84 Bargmann C, Newsome W. Brain Research through Advancing Innovative Neurotechnologies (BRAIN) Working Group. Report to the Advisory Committee to the Director, NIH 2014 Available at http://www.braininitiative.nih.gov/2025/BRAIN2025.pdf.

85 Shapiro MG, Frazier SJ, Lester HA. Unparalleled control of neural activity using orthogonal pharmacogenetics. *ACS Chemical Neuroscience* 2012; **3**: 619–629.

86 Sommakia S, Lee HC, Gaire J *et al*. Materials approaches for modulating neural tissue responses to implanted microelectrodes through mechanical and biochemical means. *Current Opinions on Solid State Material Science* 2014; **18**: 319–328.

87 Kozai TDY, Marzullo TC, Hooi F *et al*. Reduction of neurovascular damage resulting from microelectrode insertion into the cerebral cortex using *in vivo* two-photon mapping. *Journal of Neural Engineering* 2010; **7**: 46011.

88 Bjornsson CS, Oh SJ, Al-Kofahi Y a *et al*. Effects of insertion conditions on tissue strain and vascular damage during neuroprosthetic device insertion. *Journal of Neural Engineering* 2006; **3**: 196–207.

89 Biran Roy, Dave C. Martin and PAT. The brain tissue response to implanted silicon microelectrode arrays is increased when the device is tethered to the skull. *Journal of Biomedical Materials Research Part A* 2007; **82**: 169–178.

90 Christensen MB, Pearce SM, Ledbetter NM *et al*. The foreign body response to the Utah slant electrode array in the cat sciatic nerve. *Acta Biomaterialia* 2014; **10**: 4650–4660.

91 Helton KL, Ratner BD, Wisniewski NA. Biomechanics of the sensor-tissue interface—effects of motion, pressure, and design on sensor performance and the foreign body response—Part I: theoretical framework. *Journal of Diabetes Science Technology* 2011; **5**: 632–646.

92 Gilletti A, Muthuswamy J. Brain micromotion around implants in the rodent somatosensory cortex. *Journal of Neural Engineering* 2006; **3**: 189.

93 Muthuswamy J, Anand S, Sridharan A. Adaptive movable neural interfaces for monitoring single neurons in the brain. *Frontiers in Neuroscience* 2011; **5**: 94.

94 Stice P, Muthuswamy J. Assessment of gliosis around moveable implants in the brain. *Journal of Neural Engineering* 2009; **6**: 46004.

95 Tsai PS, Kaufhold JP, Blinder P *et al*. Correlations of neuronal and microvascular densities in murine cortex revealed by direct counting and colocalization of nuclei and vessels. *Journal of Neuroscience* 2009; **29**: 14553–14570.

96 Szarowski DH, Andersen MD, Retterer S *et al*. Brain responses to micro-machined silicon devices. *Brain Research* 2003; **983**: 23–35.

97 Fawcett JW, Asher Ra. The glial scar and central nervous system repair. *Brain Research Bulletin* 1999; **49**: 377–391.

98 Seymour JP, Kipke DR. Neural probe design for reduced tissue encapsulation in CNS. *Biomaterials* 2007; **28**: 3594–3607.

99 Skousen JL, Meriam ME, Srivannavit O *et al*. Reducing surface area while maintaining implant penetrating profile lowers the brain foreign body response to chronically implanted planar silicon microelectrode arrays. *Progress in Brain Research* 2011; **194**: 167.

100 Kozai TDY, Vazquez AL, Weaver CL. *In vivo* two-photon microscopy reveals immediate microglial reaction to implantation of microelectrode through extension of processes. *Journal of Neural Engineering* 2012; **9**: 1–17.

101 Kozai TDY, Langhals NB, Patel PR *et al*. Ultrasmall implantable composite microelectrodes with bioactive surfaces for chronic neural interfaces. *Nature Materials* 2012; **11**: 1065–1073.

102 Wise KD, Sodagar AM, Yao Y *et al*. Microelectrodes, microelectronics, and implantable neural microsystems. *Proceedings of the IEEE* 2008; **96**: 1184–1202.

103 Perlin GE. A Fully-implantable Integrated Front-end for Neural Recording Microsystems. ProQuest, 2008.

104 Merriam SME. A three-dimensional bidirectional interface for neural mapping studies. [Doctoral dissertation]. University of Michaigan, 2010.

105 Liu J, Fu T-M, Cheng Z *et al*. Syringe-injectable electronics. *Nature Nanotechnology* 2015; **10**: 629–636.

106 Sullivan D, Csicsvari J, Mizuseki K *et al*. Relationships between hippocampal sharp waves, ripples, and fast gamma oscillation: Influence of dentate and entorhinal cortical activity. *Journal of Neuroscience* 2011; **31**: 8605–8616.

107 McCarthy PT, Otto KJ, Rao MP. Robust penetrating microelectrodes for neural interfaces realized by titanium micromachining. *Biomedical Microdevices* 2011; **13**: 503–515.

108 Varney MW, Aslam DM, Janoudi A *et al*. Polycrystalline-diamond MEMS biosensors including neural microelectrode-arrays. *Biosensors* 2011; **1**: 118–133.

109 Lee J, Ozden I, Song Y-K *et al*. Transparent intracortical microprobe array for simultaneous spatiotemporal optical stimulation and multichannel electrical recording. *Nature Methods* 2015; **12**: 1157–1162.

110 Gabriel G, Erill I, Caro J *et al*. Manufacturing and full characterization of silicon carbide-based multi-sensor micro-probes for biomedical applications. *Microelectronics Journal* 2007; **38**: 406–415.

111 Takeuchi S, Ziegler D, Yoshida Y *et al*. Parylene flexible neural probes integrated with microfluidic channels. *Lab on a Chip* 2005; **5**: 519–523.

112 Seymour JP, Langhals NB, Anderson DJ *et al*. Novel multi-sided, microelectrode arrays for implantable neural applications. *Biomedical Microdevices* 2011; **13**: 441–451.

113 Fernández LJ, Altuna A, Tijero M *et al*. Study of functional viability of SU-8-based microneedles for neural applications. *Journal of Micromechanics and Microengineering* 2009; **19**: 25007.

114 Takeuchi S, Suzuki T, Mabuchi K *et al*. 3D flexible multichannel neural probe array. *Journal of Micromechanics and Microengineering* 2004; **14**: 104.

115 Cheung KC, Renaud P, Tanila H *et al*. Flexible polyimide microelectrode array for *in vivo* recordings and current source density analysis. *Biosensors and Bioelectronics* 2007; **22**: 1783–1790.

116 Minev IR, Musienko P, Hirsch A *et al*. Electronic dura mater for long-term multimodal neural interfaces. *Science* 2015; **347**: 159–163.

117 Karlsson JM, Haraldsson T, Carlborg CF *et al*. Fabrication and transfer of fragile 3D PDMS microstructures. *Journal of Micromechanics and Microengineering* 2012; **22**: 85009.

118 Gao J, Guo D, Santhanam S *et al*. Release and transfer of large-area ultra-thin PDMS. 2014 IEEE 27th International Conference on Micro Electro Mechanical Systems (MEMS); 26–30 Jan 2014; San Francisco, CA, USA; 2014: 544–547.

119 Wang Y, Bachman M, Li G-P. Electrodeposition of polyurethane adhesive for MEMS application. Proceedings of International Symposium on Advanced Packaging Materials: Processes, Properties and Interfaces; 16–18 Mar 2005; Irvine, CA, USA; 2005: 82–84.

120 Engel JM, Chen J, Bullen D *et al*. Polyurethane rubber as a MEMS material: Characterization and demonstration of an all-polymer two-axis artificial hair cell flow sensor. 18th IEEE International Conference on Micro Electro Mechanical Systems (MEMS 2005); 30 Jan–3 Feb 2005; Miami, FL, USA; 2005: 279–282.

121 Prange MT, Margulies SS. Regional, directional, and age-dependent properties of the brain undergoing large deformation. *Journal of Mechanical Engineering* 2002; **124**: 244–252.

122 Sridharan A, Nguyen JK, Capadona JR *et al*. Compliant intracortical implants reduce strains and strain rates in brain tissue *in vivo*. *Journal of Neural Engineering* 2015; **12**: 36002.

123 Wu F, Tien LW, Chen F *et al*. Silk-backed structural optimization of high-density flexible intracortical neural probes. *Journal of Microrlectrochemical Systems* 2015; **24**: 62–69.

124 Subbaroyan J, Martin DC, Kipke DR. A finite-element model of the mechanical effects of implantable microelectrodes in the cerebral cortex. *Journal of Neural Engineering* 2005; **2**: 103.

125 Wagner S, Lacour SP, Jones J *et al*. Electronic skin: architecture and components. *Physica E Low-dimensional Systems and Nanostructures* 2004; **25**: 326–334.

126 Kim D, Rogers JA. Stretchable electronics: materials strategies and devices. *Advanced Materials* 2008; **20**: 4887–4892.

127 Lacour SP, Chan D, Wagner S *et al*. Mechanisms of reversible stretchability of thin metal films on elastomeric substrates. *Applied Physics Letters* 2006; **88**: 204103.

128 Noh J-S. Highly conductive and stretchable poly (dimethylsiloxane): poly (3, 4-ethylenedioxythiophene): poly (styrene sulfonic acid) blends for organic interconnects. *RSC Advances* 2014; **4**: 1857–1863.

129 Secor EB, Prabhumirashi PL, Puntambekar K *et al*. Inkjet printing of high conductivity, flexible graphene patterns. *Journal of Physical Chemistry Letters* 2013; **4**: 1347–1351.

130 Rahimi R, Ochoa M, Yu W *et al*. A sewing-enabled stitch-and-transfer method for robust, ultra-stretchable, conductive interconnects. *Journal of Micromechanics and Microengineering* 2014; **24**: 95018.

131 Kim D-H, Viventi J, Amsden JJ *et al*. Dissolvable films of silk fibroin for ultrathin conformal bio-integrated electronics. *Nature Materials* 2010; **9**: 511–517.

132 Ruther P, Herwik S, Kisban S *et al*. Recent progress in neural probes using silicon MEMS technology. *IEEE Journal of Transactions on Electrical and Electronic Engineering* 2010; **5**: 505–515.

133 Oliveros A, Guiseppi-Elie A, Saddow SE. Silicon carbide: A versatile material for biosensor applications. *Biomedical Microdevices* 2013; **15**: 353–368.

134 Guitchounts G, Markowitz JE, Liberti WA *et al*. A carbon-fiber electrode array for long-term neural recording. *Journal of Neural Engineering* 2013; **10**: 46016.

135 Cogan SF. Neural stimulation and recording electrodes. *Annual Review of Biomedical Engineering* 2008; **10**: 275–309.

136 Schendel AA, Eliceiri KW, Williams JC. Advanced materials for neural surface electrodes. *Current Opinion in Solid State & Materials Science* 2014; **18**: 301–307.

137 Dadarlat MC, O'Doherty JE, Sabes PN. A learning-based approach to artificial sensory feedback leads to optimal integration. *Nature Neuroscience* 2015; **18**: 138–144.

138 Lempka SF, Johnson MD, Moffitt MA *et al*. Theoretical analysis of intracortical microelectrode recordings. *Journal of Neural Engineering* 2011; **8**: 45006.

139 Weiland JD, Anderson DJ, Humayun MS. *In vitro* electrical properties for iridium oxide versus titanium nitride stimulating electrodes. *IEEE Transactions on Biomedical Engineering* 2002; **49**: 1574–1579.

140 Negi S, Bhandari R, Rieth L *et al*. *In vitro* comparison of sputtered iridium oxide and platinum-coated neural implantable microelectrode arrays. *Biomedical Materials* 2010; **5**: 15007.

141 Millar J, Williams GV. Ultra-low noise silver-plated carbon fibre microelectrodes. *Journal of Neuroscience Methods* 1988; **25**: 59–62.

142 Ludwig KA, Uram JD, Yang J *et al*. Chronic neural recordings using silicon microelectrode arrays electrochemically deposited with a poly(3,4-ethylene-dioxythiophene) (PEDOT) film. *Journal of Neural Engineering* 2006; **3**: 59–70.

143 Gerwig R, Fuchsberger K, Schroeppel B *et al*. PEDOT–CNT composite microelectrodes for recording and electrostimulation applications: Fabrication, morphology, and electrical properties. *Frontiers in Neuroengineering* 2012; **5**: 8.

144 Venkatraman S, Hendricks J, King ZA *et al*. *In vitro* and *in vivo* evaluation of PEDOT microelectrodes for neural stimulation and recording. *IEEE Transactions on Neural Systems and Rehabilitation Engineering* 2011; **19**: 307–316.

145 Chung T, Wang JQ, Wang J *et al*. Electrode modifications to lower electrode impedance and improve neural signal recording sensitivity. *Journal of Neural Engineering* 2015; **12**: 56018.

146 Logothetis NK, Augath M, Murayama Y *et al*. The effects of electrical microstimulation on cortical signal propagation. *Nature Neuroscience* 2010; **13**: 1283–1291.

147 Huber D, Petreanu L, Ghitani N *et al*. Sparse optical microstimulation in barrel cortex drives learned behaviour in freely moving mice. *Nature* 2008; **451**: 61–64.

148 Butovas S, Schwarz C. Spatiotemporal effects of microstimulation in rat neocortex: A parametric study using multielectrode recordings. *Journal of Neurophysiology* 2003; **90**: 3024–3039.

149 Buchen L. Neuroscience: Illuminating the brain. *Nature* 2010; **465**: 26–28.

150 Ishizuka T, Kakuda M, Araki R *et al*. Kinetic evaluation of photosensitivity in genetically engineered neurons expressing green algae light-gated channels. *Neuroscience Research* 2006; **54**: 85–94.

151 Li X, Gutierrez DV, Hanson MG *et al*. Fast noninvasive activation and inhibition of neural and network activity by vertebrate rhodopsin and green algae channelrhodopsin. *Proceedings of the National Academy of Sciences of the United States of America* 2005; **102**: 17816–17821.

152 Nagel G, Brauner M, Liewald JF *et al*. Light activation of Channelrhodopsin-2 in excitable cells of caenorhabditis elegans triggers rapid behavioral responses. *Current Biology* 2005; **15**: 2279–2284.

153 Zhang F, Wang L-P, Brauner M *et al*. Multimodal fast optical interrogation of neural circuitry. *Nature* 2007; **446**: 633–639.

154 Gradinaru V, Zhang F, Ramakrishnan C *et al*. Molecular and cellular approaches for diversifying and extending optogenetics. *Cell* 2010; **141**: 154–165.

155 Allen BD, Singer AC, Boyden ES. Principles of designing interpretable optogenetic behavior experiments. *Learning & Memory* 2015; **22**: 232–238.

156 Buzsáki G, Stark E, Berényi A *et al*. Tools for probing local circuits: High-density silicon probes combined with optogenetics. *Neuron* 2015; **86**: 92–105.

157 Adamantidis A, Arber S, Bains JS *et al*. Optogenetics: 10 years after ChR2 in neurons-views from the community. *Nature Neuroscience* 2015; **18**: 1202.

158 Prakash R, Yizhar O, Grewe B *et al*. Two-photon optogenetic toolbox for fast inhibition, excitation and bistable modulation. *Nature Methods* 2012; **9**: 1171–1179.

159 Anikeeva P, Andalman AS, Witten I *et al*. Optetrode: A multichannel readout for optogenetic control in freely moving mice. *Nature Neuroscience* 2011; **15**: 163–170.

160 Zorzos AN, Boyden ES, Fonstad CG. Multiwaveguide implantable probe for light delivery to sets of distributed brain targets. *Optics Letters* 2010; **35**: 4133–4135.

161 Stark E, Roux L, Eichler R *et al*. Pyramidal cell-interneuron interactions underlie hippocampal ripple oscillations. *Neuron* 2014; **83**: 467–480.

162 Wu F, Stark E, Im M *et al*. An implantable neural probe with monolithically integrated dielectric waveguide and recording electrodes for optogenetics applications. *Journal of Neural Engineering* 2013; **10**: 056012.

163 Im M, Cho I-J, Wu F *et al*. A dual-shank neural probe integrated with double waveguides on each shank for optogenetic applications. Annual International Conference of the IEEE Engineering in Medicine and Biology Society 2011; 30 Aug–3 Sep 2011; Boston, MA, USA; 2011: 5480–5483.

164 Im M, Cho I, Wu F *et al*. Neural probes integrated with optical mixer/splitter waveguides and multiple stimulation sites. MEMS; Cancun, Mexico; 2011: 1051–1054.

165 Schwaerzle M, Seidl K, Schwarz UT *et al*. Ultracompact optrode with integrated laser diode chips and SU-8 waveguides for optogenetic applications. IEEE 26th International Conference on Micro Electro Mechanical Systems (MEMS); 20–24 Jan 2013; Taipei, China; 2013: 1029–1032.

166 Kampasi K, Seymour JP, Na K *et al*. Fiberless multicolor optoelectrodes using injection laser diodes and gradient-index lens coupled optical waveguides. Transducers' 15; 21–25 Jun 2015; Anchorage, AK, USA; 2015: 273–276.

167 Kampasi K, Stark E, Seymour J *et al*. Fiberless multicolor neural optoelectrode for *in vivo* circuit analysis. *Scientific Reports* 2016; **6**: 30961.

168 Aravanis AM, Wang L-P, Zhang F *et al*. An optical neural interface: *In vivo* control of rodent motor cortex with integrated fiberoptic and optogenetic technology. *Journal of Neural Engineering* 2007; **4**: S143–S156.

169 Adamantidis AR, Zhang F, de Lecea L *et al*. Optogenetics: Opsins and optical interfaces in neuroscience. *Cold Spring Harbor Protocol* 2014; **8**: 815–822.

170 Stujenske JM, Spellman T, Gordon JA. Modeling the spatiotemporal dynamics of light and heat propagation for *in vivo* optogenetics. *Cell Report* 2015; **12**: 525–534.

171 Bernstein JG, Garrity PA, Boyden ES. Optogenetics and thermogenetics: technologies for controlling the activity of targeted cells within intact neural circuits. *Current Opinions in Neurobiology* 2012; **22**: 61–71.

172 Nakamura S, Senoh M, Iwasa N. Nagahama S-I. High-brightness in InGaN blue, green and yellow light-emitting diodes with quantum well structures. *Japanese Journal of Applied Physics, Part 2 Letters* 1995; **34**: 797–799.

173 Lee JH, Lee DY, Oh BW *et al*. Comparison of InGaN-based LEDs grown on conventional sapphire and cone-shape-patterned sapphire substrate. *IEEE Transactions on Electron Devices* 2010; **57**: 157–163.

174 Mcalinden N, Massoubre D, Richardson E *et al*. Thermal and optical characterization of micro-LED probes for *in vivo* optogenetic neural stimulation. *Optics Letters* 2013; **38**: 992–994.

175 Kim T-IT, McCall JG, Jung YH *et al*. Injectable, cellular-scale optoelectronics with applications for wireless optogenetics. *Science* 2013; **340**: 211–216.

176 Wu F, Stark E, Ku P-C *et al*. Monolithically integrated µLEDs on silicon neural probes for high-resolution optogenetic studies in behaving animals. *Neuron* 2015; **88**: 1136–1148.

177 Harris JJ, Jolivet R, Attwell D. Synaptic energy use and supply. *Neuron* 2012; **75**: 762–777.

178 Scholvin J, Kinney J, Bernstein J *et al*. Close-packed silicon microelectrodes for scalable spatially oversampled neural recording. *IEEE Transactions on Biomedical Engineering* 2015; **63**: 120–130.

179 Lopez CM, Mitra S, Putzeys J *et al*. 22.7 A 966-electrode neural probe with 384 configurable channels in 0.13µm SOI CMOS. 2016 IEEE International Solid-State Circuits Conference (ISSCC); 29 Oct–4 Nov 2006; San Diego, CA, USA; 2016: 392–393.

180 Pajouhi H, Jou AY, Jain R *et al*. Flexible complementary metal oxide semiconductor microelectrode arrays with applications in single cell characterization. *Applied Physics Letters* 2015; **107**: 203103.

16

181 Park S-Y, Cho J, Na K *et al.* Toward 1024-channel parallel neural recording: modular δ-δσ analog front-end architecture with 4.84fj/c-s-mm² energy-area product. Symposium on VLSI Circuits (VLSIC) 2015; 17–19 Jun 2015; Kyoto, Japan; 2015: C112–C113.

182 Perlin GE, Wise KD. An ultra compact integrated front end for wireless neural recording microsystems. *Journal of Microrlectrochemical Systems* 2010; **19**: 1409–1421.

183 Ballini M, Muller J, Livi P *et al.* A 1024-Channel CMOS microelectrode array with 26,400 electrodes for recording and stimulation of electrogenic cells *in vitro. IEEE Journal on Solid-State Circuits* 2014; **49**: 2705–2719.

184 Johnson B, Peace ST, Cleland TA *et al.* A 50μm pitch, 1120-channel, 20kHz frame rate microelectrode array for slice recording. 2013 IEEE Biomedical Circuits and Systems Conference (BioCAS); 31 Oct–2 Nov 2013; Rotterdam, The Netherlands; 2013: 109–112.

185 Manghisoni M, Ratti L, Re V *et al.* Noise characterization of 130 nm and 90 nm CMOS technologies for analog front-end electronics. 2006 IEEE Nuclear Science Symposium Conference Record; 29 Oct–4 Nov 2006; San Diego, CA, USA; 2006: 214–218.

186 Re V, Manghisoni M, Ratti L *et al.* Survey of noise performances and scaling effects in deep submicron CMOS devices from different foundries. 2004 IEEE Nuclear Science Symposium Conference Record; 16–22 Oct 2004; Rome, Italy; 2004: 1368–1372.

187 Muller R, Gambini S, Rabaey JM. A 0.013, 5, DC-coupled neural signal acquisition IC with 0.5 V supply. *IEEE Journal of Solid-State Circuits* 2012; **47**: 232–243.

188 Frey U, Heer F, Pedron R *et al.* Switch-matrix-based high-density microelectrode array in CMOS technology. *IEEE Journal of Solid-State Circuits* 2010; **45**: 467–482.

189 Shahrokhi F, Abdelhalim K, Serletis D *et al.* The 128-channel fully differential digital integrated neural recording and stimulation interface. *IEEE Transactions on Biomedical Circuits and Systems* 2010; **4**: 149–161.

190 Fischer AC, Forsberg F, Lapisa M *et al.* Integrating MEMS and ICs. *Microsystems and Nanoengineering* 2015; **1**: 15005.

191 Liu D, Park S. Three-dimensional and 2.5 dimensional interconnection technology: state of the art. *Journal of Electronic Packaging* 2014; **136**: 14001.

192 Meyer J-U, Stieglitz T, Scholz O *et al.* High density interconnects and flexible hybrid assemblies for active biomedical implants. *IEEE Transactions on Advance Packaging* 2001; **24**: 366–374.

193 Ohara Y, Noriki A, Sakuma K *et al.* 10 μm fine pitch Cu/Sn micro-bumps for 3D super-chip stack. IEEE International Conference on 3D System Integration 2009 (3DIC 2009); 28–30 Sep 2009; San Francisco, CA, USA; 2009: 1–6.

194 Xie X, Rieth L, Williams L *et al.* Long-term reliability of Al_2O_3 and Parylene C bilayer encapsulated Utah electrode array based neural interfaces for chronic implantation. *Journal of Neural Engineering* 2014; **11**: 26016.

195 Haque R-U, Wise KD. A glass-in-silicon reflow process for three-dimensional microsystems. *Journal of Microelectromechanical Systems* 2013; **22**: 1470–1477.

196 Lee S-H, Mitchell J, Welch W *et al.* Wafer-level vacuum/hermetic packaging technologies for MEMS. *Proceedings of SPIE* 2010; 759205.

197 Deisseroth K, Schnitzer MJ. Engineering approaches to illuminating brain structure and dynamics. *Neuron* 2013; **80**: 568–577.

198 Samara A. Single neurons needed for brain asymmetry studies. *Frontiers in Genetics* 2013; **4**: 311.